Proposal for PAC 31
Draft 0

Meson spectroscopy in the Coherent Production on ^{4}He with CLAS

Search for Exotic Hybrids

G. Asryan, I. Aznauryan,[1] N. Dashyan, N. Gevorgyan
Yerevan Physics Institute, Yerevan, Armenia

M. Amaryan, S. Bueltman, G. Dodge, S. Kuhn, L. Weinstein, J. Zhang
Old Dominion University, Norfolk, VA, USA

V. Burkert, D.S. Carman, L. Elouadrhiri, H. Fenker,[1] A. Freyberger,
L. Guo, R. Niyazov, E. Smith, S. Stepanyan,[1,2] D. Weygand
Jefferson Lab, Newport News, VA, USA

C. Salgado[1] and M. Khandaker
Norfolk State University, Norfolk, VA, USA

C. Bookwalter, P. Eugenio[1], A. Ostrovidov
Florida State University, Tallahassee, FL, USA

V. Kubarovsky and P. Stoler
Rensselaer Polytechnic Institute, Troy, NY, USA

K. Griffioen and N. Baillie
College of William and Mary, Williamsburg, VA, USA

J. Ball and M. Garçon
CEA-Saclay, Service de Physique Nucléaire, 91191 Gif-sur-Yvette, France

G.P. Gilfoyle
University of Richmond, Richmond, VA, USA

K. Hicks and T. Mibe
Ohio University, Athens, OH, USA

H. Egiyan and M. Holtrop
University of New Hampshire, Durham, NH, USA

R. Gothe and S. Strauch
University of South Carolina, Columbia, SC, USA

[1] Co-Spokesperson
[2] Contact-person

B.L. Berman, W. Briscoe, Y. Ilieva, I. Strakovsky
The George Washington University, Washington, DC, USA

D. Jenkins
Virginia Polytechnic Institute and State University, Blacksburg, VA, USA

M. Battaglieri and R. De Vita
INFN, Sezione di Genova, Genova, Italy

O. Pogorelko
ITEP, Moscow, Russia

and the CLAS Collaboration

Abstract

This experiment will search for $J^{PC} = 1^{-+}$ exotic hybrids in the $\pi\eta$ and $\pi\eta'$ decay modes, using quasi-real photoproduction on ^{4}He. Coherent production of t-channel mesons, when the recoiling nuclei stay intact, is a powerful method to eliminate physics background from s-channel processes. In addition, scattering off a spin- and isospin-zero target, ^{4}He, will simplify significantly the PWA. The quantum numbers C and G of the produced meson will be determined by the identification of its decay products. Final states $\pi^0\eta$ and $\pi^0\eta'$ have $G = -1$, $C = +1$ and $P = (-1)^L$, where L is the angular momentum of the produced pair. $L = 1$ gives exotic quantum numbers $I^G J^{PC} = 1^-1^{-+}$. A determination of $J(= L)$ and, therefore, P will be done via analysis of the decay angular distribution of the final state meson in a PWA.

The experiment will use a 6 GeV electron beam and the CLAS detector to search for exotic states in the mass range up to 2 GeV. We will use the standard CLAS detector package, with the DVCS solenoid magnet, the BoNuS RTPC with a high pressure ^{4}He gas target, and the DVCS $PbWO_4$ crystal calorimeter. A forward (post target) tagging system will be built to detect scattered electrons at very small angles, which is important for detector calibration and systematic checks. We request 45 days of beam time for this experiment.

The present proposal was submitted as a letter-of-intent to PAC23 in 2003. At that time numerous discussions with PAC members took place. Particularly, the discussions with Prof. Donnachie were extremely productive and helpful to shape the present proposal. We were encouraged by PAC to submit a full proposal, which we are doing now. Below, is the full PAC23 report on the letter-of-intent. We met all of the recommendations that PAC23 made.

PAC23 report on the LOI 03003
"Search for Exotic Hybrids in the Coherent Production off ^{4}*He"*
Contact Person: S. Stepanyan

The LOI proposes to search for mesons with exotic quantum numbers, the $\pi_1(1400)$ *and the* $\pi_1(1600)$*, in the* $\pi^0\eta$ *and* $\pi^0\eta'$ *channels using coherent production with quasireal photons on* ^{4}*He. Additionally the C(1480) will be studied in the* $\phi\pi^0$ *channel. Coherent production has several advantages, including no background from baryon resonances and, at* $t = t_{min}$*, no helicity flip so that the helicity of the* $\pi^0\eta$ *and* $\pi^0\eta'$ *will be the same as that of the initial photon. It is assumed that this latter condition will hold for* $|t| > |t_{min}|$ *thus simplifying the partial wave analysis of the final state. It is also assumed that the reactions are dominated by natural parity exchange. The use of an electron beam instead of a tagged photon beam has several advantages but does require the construction of a forward electron tagger.*

The Collaboration is encouraged to return with a full proposal addressing the following issues.

1. *It should be demonstrated that the assumptions of no helicity flip and natural parity exchange are not necessary for the partial wave analysis. (Addressed in Section 4)*

2. *The estimate of cross sections should be clarified and the assumptions going into that estimate justified. (Addressed in Section 5)*

3. *Separate rate estimates should be made for the* $\pi_1(1400)$ *and the* $\pi_1(1600)$*. (Addressed in Section 5)*

4. *The technical feasibility of the forward electron tagger and* ^{4}*He tagging should be established. (Addressed in Section 7)*

5. *The viability of the experiment without tagging the electron should be evaluated. (Addressed in Section 7)*

Contents

1 Introduction

High energy experiments have provided clear evidence for significant contributions of gluons to hadron structure. Evidence for gluons has been found in jet measurements and in deep inelastic scattering. However there is almost complete lack of knowledge of the properties of soft gluon. Soft gluons must certenly be understood is phenomena such as color confinment, mass generation, and dynamical symmetry breaking are to be understood. The discovery and explication of hadrons with gluonic degrees of freedom (hybrids) is clearly an important step in this process.

QCD models have made a variety of predictions for the masses, widths, and decay modes of hybrid $gq\overline{q}$ states [1, 2, 3, 4, 5, 6, 7, 8, 9]. The predicted mass of the lowest lying hybrid is $\leq$ 2 GeV. The best way, perhaps the only way, to search for hybrid states in this mass region is to look for states with exotic quantum numbers, i.e. quantum numbers not accessible for $q\overline{q}$, since this region is densely populated with ordinary $q\overline{q}$ states and non-exotic hybrids will mix with ordinary mesons. A bound system consisting of only a fermion - anti-fermion pair, i.e., a $q\overline{q}$ system, lacks some members of its $J \geq 1$ natural spin-parity states (i.e., $J^P = 1^-;\ 2^+;\ 3^-;\ 4^+$). For neutral mesons, states with $P \neq C$ will be lacking. In contrast, a constituent boson added to a $q\overline{q}$ pair will allow "spin-parity" exotic quantum numbers (e.g. $J^{PC} = 1^{-+};\ 2^{+-};\ 3^{-+};\ 4^{+-}$).

Most of the searches for exotics have used hadronic production reactions, i.e. πN and $p\bar{p}(n)$, characteristically yielding high statistics. J/ψ decays have been studied as well, but with considerably lower statistics. So far two states below 1.8 GeV have been identified as $J^{PC} = 1^{-+}$ exotics at masses around 1.4 GeV and 1.6 GeV (see discussions below). It is not clear if these are hybrids or four-quark states, and there is a controversy in the amplitude analysis. For clarification, more experiments in different production and/or decay modes, with high statistics and robust amplitude analyses are needed.

We propose to search for exotic states with $I^G J^{PC} = 1^-1^{-+}$ in the mass range $m <$ 2 GeV using coherent quasi-real photoproduction of $\pi^0\eta$ and $\pi^0\eta'$ final states on ^{4}He. **Coherent production of mesonic states off nuclei eliminates background arising from the production of baryon resonances. Baryon resonances are the source of the main and significant background to the t-channel processes leading to the production of exotic mesons. A large contribution of baryon resonances makes PWA analysis very complicated. Suppression of this contribution is the key feature of the proposed measurements. In addition, coherent production off a spin- and isospin-zero ($S = 0$ and $I = 0$) target will significantly simplify the partial-wave analysis (PWA) [10].** The measurements will be carried out using the CLAS detector in Hall B and a 6 GeV electron beam at Jefferson Lab. Final states $\pi^0\eta$ and $\pi^0\eta'$ have $G = -1$, $C = +1$ and $P = (-1)^L$, where L is the angular momentum of the produced pair. $L = 1$

gives the exotic quantum numbers $I^G J^{PC} = 1^- 1^{-+}$. A determination of $J(= L)$ and, therefore, P, will be done via analysis of the angular distribution of the π^0, η, and η' mesons in a PWA.

2 Physics Motivation

Perhaps the most fundamental question of interest to hadron physicists is that of understanding the mechanism of confinement. It has been more than thirty years since QCD was postulated as the theory of strong interactions. While much progress has been made in understanding perturbative phenomena, the non-perturbative regime, the regime of hadrons, their excitations, and their couplings, has remained largely impervious to our varied assaults. Only recently, with improvements of lattice QCD calculations, it has become possible to make predictions of the spectrum of hadrons [11, 12] directly from QCD, based on very few parameters (such as the bare quark masses). New experimental efforts to determine the hadron spectra are timely and are important for progress in non-perturbative QCD.

Gluonic excitations of mesons with "exotic" quantum numbers would be the most direct evidence for states beyond the quark model. Determining the properties of such states through studies via different production and decay mechanisms would shed light on the QCD confinement mechanism.

The goal of a large part of the JLab physics program at 12 GeV is to map out the spectrum of mesons in the light quark sector with an emphasis on the search for gluonic excitations (GlueX program in Hall D). This proposed experiment therefore represents an exciting opportunity to explore the photoproduction landscape and to provide feedback to the 12 GeV program regarding exotic signatures and background.

The mass range of the lowest lying exotic hybrid is accessible at current CEBAF energies. The CLAS detector is an ideal tool for studying multi-particle final states. There is already one completed experiment on the search for exotic mesons in photoproduction off hydrogen, and the first results are very encouraging [13]. The second experiment on hydrogen with up to 6 GeV photons is in the queue [14]. However both measurements require complex Partial Wave Analysis (PWA) to disentangle t-channel and s-channel production. In the proposed measurements, contributions from non-direct meson production will be highly suppressed. The PWA will be much simpler and therefore with much less ambiguity.

2.1 Theoretical predictions for hybrids

The existence of exotic hybrid mesons has been predicted and states have been searched for more than 3-decades (for a review see [15, 16, 17]). Almost all QCD models predict a $J^{PC} = 1^{-+}$ hybrid with a mass at or below 2 GeV [1, 2, 3, 4]. Widths in the range $\Gamma \sim 50 \rightarrow 200$ MeV are favored. The decay modes are uncertain. In the flux tube model, the gluonic excitation does not transfer its spin to the relative

orbital angular momentum of the final state mesons, and the hybrid decay to two S-wave mesons is forbidden [18, 5, 6]. However, in the case of the pion in the final state this selection rule can be violated by shrinking the π to a point-like current [7]. Other models [2, 19, 20] predict such a decay. This occurs through effects such as spurious bag CM motion [2], or through the sequential decay of the exotic hybrid into a non-exotic hybrid and then into a conventional meson via mixing [20]. The non-exotic hybrid is mixed with a conventional meson which appears in the final state. In this description, the $\pi^0\eta$ and $\pi^0\eta'$ states have small constituent gluonic components. In general, branching ratios into $\pi\eta$ and $\pi\eta'$ are predicted to be $Br_{\pi\eta} \sim 0.1$ and $Br_{\pi\eta}/Br_{\pi\eta'} \sim 1/3$.

A summary of lattice results on $J^{PC} = 1^{-+}$ exotic hybrids up to 2003 can be found in [8], where the light-quark exotic is predicted to have a mass of 1.9(2) GeV. However, the latest lattice results on the mass of the $J^{PC} = 1^{-+}$ hybrid do not contradict with the $\pi_1(1600)$ candidate. This can be seen from Fig. 1 (taken from Ref. [9]), where a summary of the existing simulations for $J^{PC} = 1^{-+}$ exotics is given. Lattice predictions for decay width span from 40 to 100 MeV, see e.g. [22]. Favorable decays are to (PS) mesons [23].

2.2 Experimental Status of J^{PC}=1^{-+} Hybrids

While the current results from lattice QCD indicate that the lightest exotic meson nonet has quantum numbers J^{PC}=1^{-+} and its lightest member, the π_1, has a mass in the range from 1.5 to 2.0 GeV, the current experimental evidence is much less clear. During the past 15 years, a number of different experiments have provided tantalizing evidence for the 1^{-+} exotics $\pi_1(1400)$, $\pi_1(1600)$, and $\pi_1(2000)$. If each of these states was verified, this would result in an overpopulation of the 1^{-+} hybrid nonet where there should be only one π_1 state. In this section we provide a brief overview on each of the reported 1^{-+} exotic candidates.

2.2.1 Evidence for the $\pi_1(1400)$

The $\pi_1(1400)$ was first reported by the GAMS group at CERN [24]. It was seen in the $\pi^- p \to \eta\pi^0 n$ channel at p_π=100 GeV. A partial wave analysis of these data showed a clear $a_2(1320)$ D-wave, and a narrow enhancement in the unnatural parity exchange P_0-wave at a mass of $\sim$1.4 GeV. The natural parity exchange P_+-wave was observed to be structureless. However, these conclusions were refuted by some of the original authors who pointed out that the $\eta\pi^0$ PWA suffered from an eight-fold ambiguity which was not properly accounted for in the analysis [10, 25].

The VES Collaboration at IHEP [26], which studied the reaction $\pi^- N \to \pi^-\eta N$ with p_π=37 GeV, reported a small but statistically significant broad enhancement in the natural parity exchange P_+-wave at about 1.4 GeV. The authors made no attempt to identify the P_+ enhancement with a resonance. Experiment E179 at KEK studied the decay angular distributions in the $\pi^- p \to \eta\pi^- p$ reaction at p_π=6.3 GeV. They

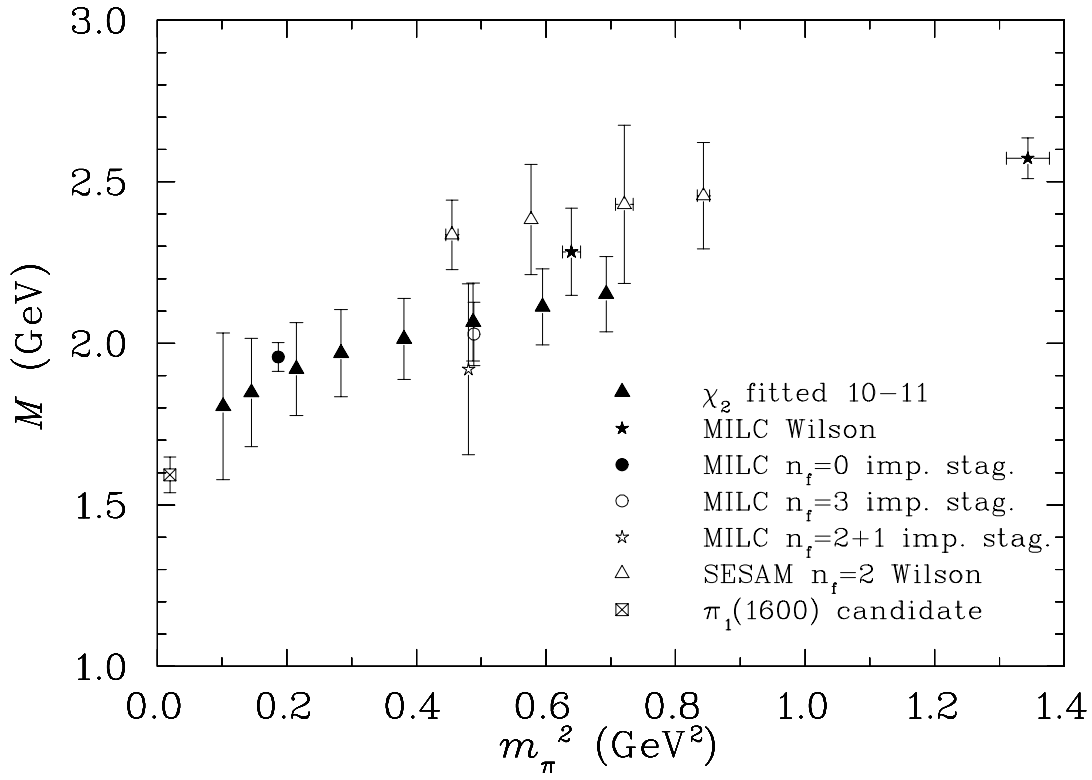

Figure 1: A survey of LQCD results. Here the mass of $J^{PC} = 1^{-+}$ exotic state is plotted vs. the pion mass squared (m_π^2). The open and closed symbols denote dynamical and quenched simulations respectively. The MILC results are taken from [21].

observed an enhancement around 1.3 GeV in the P_+-wave but find that they were unable to establish a resonant nature. They noted the phase of the P_+-wave relative to the D_+ $a_2(1320)$ wave showed no distinct variation with mass [27].

A second generation of experiments then followed these early efforts. Observation and first resonant claim of the $\pi_1(1400)$ was provided by the E852 Collaboration at BNL in the reactions $\pi^- p \to \eta\pi^0 n$ and $\pi^- p \to \eta\pi^- p$ at p_π=18 GeV [28]. In this analysis the resonant nature of the P_+-wave arises from a strong interference with the D_+ $a_2(1320)$ wave. The phase difference between these waves exhibited a phase motion not attributable solely to the $a_2(1320)$. Results from the Crystal Barrel experiment at CERN for the reactions $\bar{p}p \to \eta\pi^0\pi^0$ and $\bar{p}n \to \eta\pi^-\pi^0$ at $p_{\bar{p}}$=200 MeV [29], needed to include a $\pi_1(1400)$ state in addition to conventional mesons to fit their data.

In the PDG listings [30], the mass of the $\pi_1(1400)$ is M=1376±17 MeV and its width Γ=300±40 MeV with observed decays to $\eta\pi^0$ and $\eta\pi^-$. However the current experimental evidence gives rise to a number of controversial issues. The $\pi_1(1400)$

is significantly lighter than theoretical expectations. It has been suggested that the $\pi_1(1400)$ could represent a meson-meson molecule. An alternative suggestion is that the $\pi_1(1400)$ could actually be a threshold effect of a higher mass π_1 resonance due to the opening of more favorable decay channels. Other recent work suggests that the exotic P-wave signature for the $\pi_1(1400)$ may actually arise from dynamical non-resonant scattering, similar to S-wave $\pi\pi$ scattering at low energy [31].

A recent analysis of E852 data by Dzierba *et al.* was focussed on an amplitude analysis of the $\eta\pi^0$ mode in three different t bins (see Fig. 2) [32]. This analysis concluded that no consistent P-wave resonant parameters can describe the data for the $\pi_1(1400)$, while the resonant parameters obtained for the $a_2(1320)$ phase reference state are consistent for the different t bins with the PDG values. However the question remains as to what causes the peaking in the P-wave intensity distributions, and if it is due to a non-resonant source, what explains the phase motion with respect to the $a_2(1320)$?

Another interesting fact is that while the exotic wave is a few percent of the dominant a_2 wave in the E852 data, it is of comparable strength to the a_2 in the Crystal Barrel results. However, each of the existing data sets in these hadroproduction experiments is hampered by relatively low statistics.

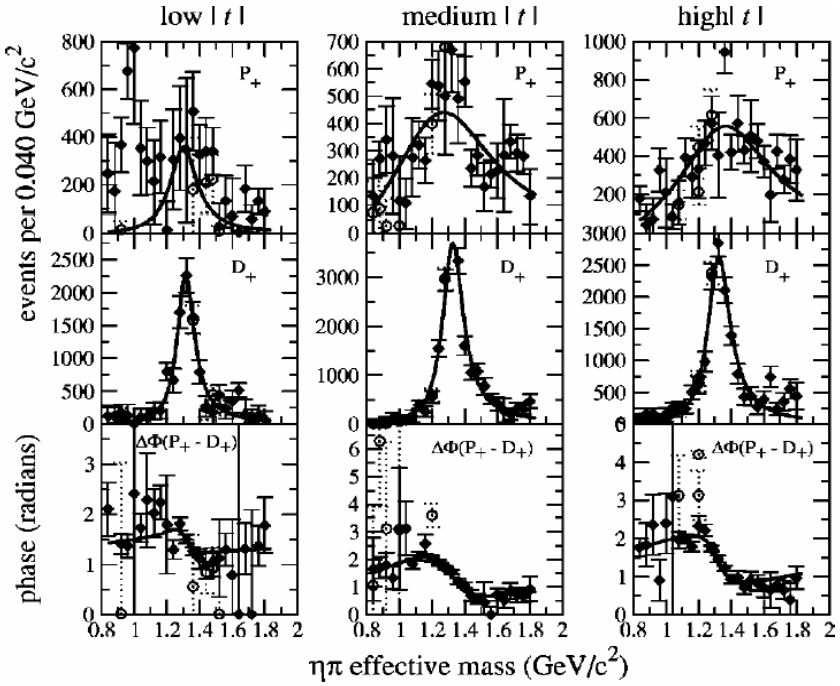

Figure 2: PWA solution for the P_+ (top) and D_+ (middle) waves, and the phase difference (bottom) for the three t bins used in the analysis as a function of the $\eta\pi^0$ effective mass [32].

2.2.2 Evidence for the $\pi_1(1600)$

A second $J^{PC} = 1^{-+}$ exotic meson at 1.6 GeV has been claimed by the BNL E852 Collaboration in the $\eta'\pi$, $\rho\pi$, $b_1\pi$, and $f_1\pi$ final states in $\pi^- p$ reactions at p_π=18 GeV [34, 38, 39, 40]. This signal first appeared as an enhancement in the P_+-wave in an early $\eta'\pi$ measurement by the VES Collaboration [26]. Additional VES measurements followed with confirmation of the $\pi_1(1600)$ decaying into $b_1\pi$, $\eta'\pi$, and $\rho\pi$ [33]. This work provided measurements of the relative branching ratios into $b_1\pi$, $\eta'\pi$, and $\rho\pi$ of 1.0:1.0:1.6. These predictions are highly at odds with predictions of the flux-tube model. Thus either these three modes are not all due to a hybrid meson or there is a problem with the amplitude analysis or the flux-tube model.

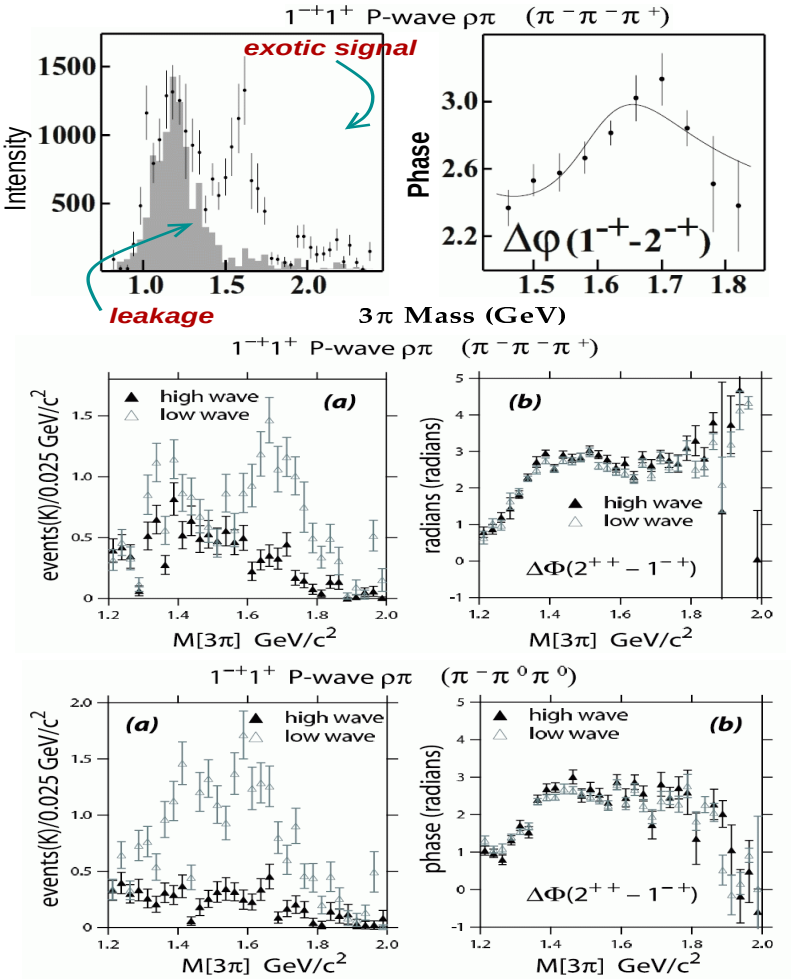

Figure 3: PWA results from analysis of E852 data for the $\pi^-\pi^-\pi^+$ channel (top and middle rows) and for the $\pi^-\pi^0\pi^0$ channel (bottom row) as a function of the 3π effective mass. The upper row of plots is from Ref. [34] and the bottom two rows are from Ref. [41].

The evidence for the $\pi_1(1600)$ from its decay into $\rho\pi$ is particularly controversial. The analysis results for the $\rho\pi$ final state are shown in Fig. 3. The top row of this

figure shows the $\rho\pi$ analysis from E852 [34] from the 1994 data run based on 250k events. Here an exotic 1^{-+} signal is reported at a mass of M=1593$\pm$8$\binom{+29}{-47}$ MeV with a width Γ=168$\pm$20$\binom{+150}{-12}$ MeV. The middle row of Fig. 3 shows analysis of the 1995 E852 data by Dzierba *et al.* [41] for $\rho\pi$ decay to $\pi^-\pi^-\pi^+$ and the bottom row shows the $\rho\pi$ decay from the 1995 data to $\pi^-\pi^0\pi^0$. This later data run had roughly four times the statistics compared to the earlier run. This work highlighted a strong PWA model dependence of the shape and magnitude of the 1^{-+} signal. The 1^{-+} intensity distribution exhibits a strong resonance-like distribution using a PWA model with a minimum number of partial waves (21 waves). However, when a larger wave set is used (denoted as the high wave set in Fig. 3 – includes 35 waves), the evidence for the $\pi_1(1600)$ in the intensity distributions is washed out. Nonetheless, it is curious that the phase motion plots are essentially unchanged between the two choices of wave sets.

The comparison of the two $(3\pi)^-$ modes provides powerful cross checks on the analysis results. Any resonance decaying to $(\rho\pi)^-$ should decay equally to $(\pi^-\pi^0)\pi^0$ and $(\pi^+\pi^-)\pi^0$, and thus appear with equal probabilities in the two modes.

In the E852 analysis of $\pi^-p \to \eta'\pi$, evidence for an exotic 1^{-+} state with a mass M=1597$\pm$10$\binom{+45}{-10}$ MeV and width Γ=340$\pm$40$\pm$50 MeV is shown [38] (see Fig. 4). It is interesting that the P-wave strength is the dominant signal in $\eta'\pi$ compared to $\rho\pi$. However, the strength in the D-wave used as the phase reference in the $\eta'\pi$ analysis is not well understood. So while there are some noted controversies associated with the $\pi_1(1600)$, there clearly are some hints from a number of experiments that need to be further investigated.

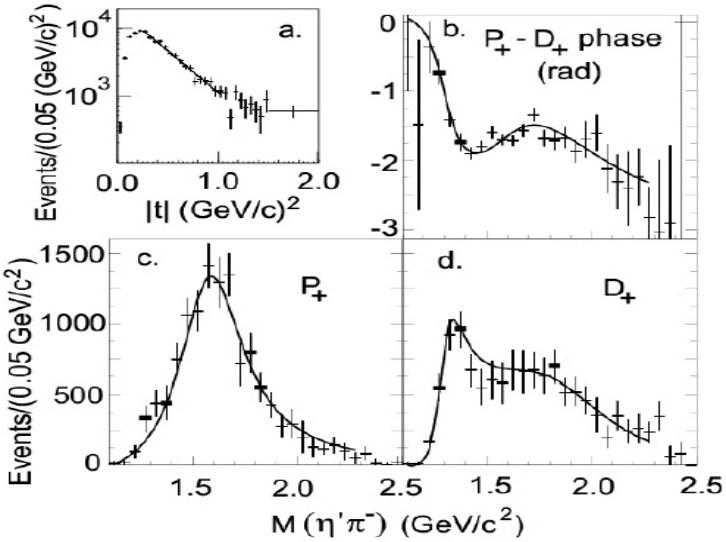

Figure 4: (a) The t-distribution of the $\eta'\pi$ data. (b)-(d) PWA results for the P_+ and D_+ waves as a function of the $\eta'\pi$ effective mass along with the results of a mass-dependent fit [38].

2.2.3 Evidence for the $\pi_1(2000)$

A final $J^{PC}=1^{-+}$ meson candidate is the $\pi_1(2000)$ which has been claimed by the E852 Collaboration through its decays into $f_1\pi$ [39] and $b_1\pi$ [40]. While this is encouraging as this state is more line with what is expected from flux tube models and the lattice calculations, the data are of relatively limited statistical accuracy. In fact the quality of the data is such that strong conclusions regarding evidence for this state cannot be made.

The reported $\pi_1(2000)$ from $f_1\pi$ was seen through the reaction $\pi^- p \to \pi^-\pi^-\pi^+\eta n$ and has a mass M=2001±30±92 MeV and width Γ=333±52±49 MeV. As seen from $b_1\pi$ through the reaction $\pi^- p \to \omega\pi^0\pi^- p$, the mass and width are quoted as M=2014±20±16 MeV and Γ=230±32±73 MeV. Note however that the mass reach of our proposed experiment will be limited by statistics above about 1.8 GeV.

Even beyond issues associated with the statistics, the different experiments are hampered by a number of analysis issues. Perhaps the most important problem arises due to leakage effects in the amplitude analysis. While the implementation of a partial wave analysis is in principle straightforward, there are difficulties that arise due to the detector system employed, as well as ambiguities within the PWA framework itself. Effects such as detector acceptance and resolution can conspire to allow strength from a dominant partial wave to appear as strength in a weaker wave. Another important issue involves the model dependent assumptions made within the PWA framework itself. In PWA, simplifying assumptions are used in order to make the fitting model more tractable, such as in calculating decay amplitudes via an isobar model, and the absolute effects of these assumptions are not fully known.

2.3 Summary of physics motivation

Since the first observation of the $\pi_1(1400)$, then called the "M" meson, its status has been controversial [24]. The original GAMS result was withdrawn [25], and subsequent observation by KEK [27] has been disputed. Results from VES [26], E852 [28], and the Crystal Barrel [29] are less controversial regarding the experimental observation, however the nature of the $\pi_1(1400)$ is not clear. Possibilities include a tetra-quark [37, 36] and a gluonic hybrid, as well as a rescattering effect [35]. The current experiment, regardless of the result, will shed light on the nature of the state. Photoproduction of a gluonic hybrid will be enhanced relative to the $a_2(1320)$, while final state interactions will be reduced in coherent production off of ^4He. The existence of the $\pi_1(1600)$ seen in the decay $\eta'\pi$ is much less controversial, while the decay to 3 pions is controversial. Efforts to observe this state in the 3 pion mode via photoproduction have not been successful. Again, the nature of this state is unknown, and a photoproduction experiment sensitive to the well established $\eta'\pi$ decay mode will provide crucial information on this exotic particle.

Given this overview with its strong hints and potential worries associated with leakage in the amplitude analysis, the proposed experiment can provide for studies of

the P-wave exotics in the mass range below about 1.8 GeV in an amplitude analysis that is subject to *very* different systematics, and is much more straightforward, clean, and under control.

3 Proposed Experiment

In this experiment we propose to search for $J^{PC} = 1^{-+}$ exotic states in the coherent production of $\pi^0\eta$ and $\pi^0\eta'$ final states off ^{4}He, using up to a 6 GeV photon beam (see Fig. 5). The advantages of studying $\pi^0\eta$ and $\pi^0\eta'$ systems in unpolarized photoproduction reactions on nuclear targets coherently was first discussed in Ref. [10]. Final states $\pi^0\eta$ and $\pi^0\eta'$ have $G = -1$, $C = +1$ and $P = (-1)^L$, where L is the angular momentum of produced pair. $L = 1$ gives exotic quantum numbers $I^G J^{PC} = 1^-1^{-+}$. A determination of $J(= L)$ and, therefore, P, will be done through analysis of the decay angular distributions of the final state mesons via a PWA.

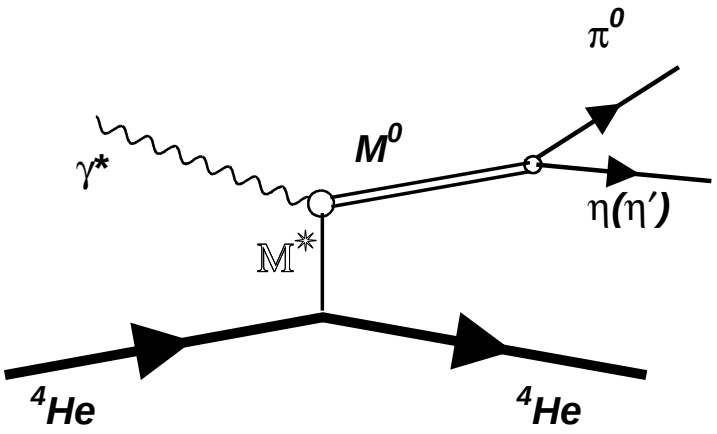

Figure 5: Coherent production of a neutral meson M^0 on ^4He with subsequent decay to $\pi^0\eta$ and $\pi^0\eta'$ final states.

The background to the electromagnetic production of meson resonances via t-channel exchanges (see Fig.6.a) arises from associated production of baryon resonances that decay into the same final state particles (see Fig.6.b) and from processes associated with the Deck effect [42, 43] (see Fig.6.c). Often final state particles in these production reactions occupy the same phase space, and therefore, it becomes impossible to separate these processes using kinematic cuts. Contributions from non-direct t-channel meson production reactions make PWA analysis rather complicated, require high event statistics, and high resolution and geometrical acceptance of the detector. The production of meson resonances coherently on nuclear targets, when the recoil nucleus remains intact, is a *clean* way to eliminate baryon resonances. A particular case of such processes is coherent production off light nuclei, *e.g.*, ^{3}H, ^{3}He,

^{4}He. In these cases the recoil nucleus can be detected in order to ensure that it remains intact.

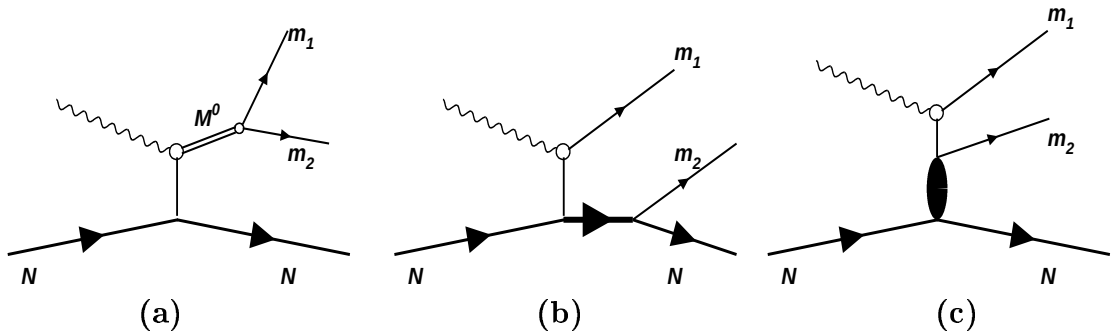

Figure 6: Diagrams contributing to the photoproduction of mesons m_1 and m_2 on a nucleon. (a) is the diagram for t-channel meson production, M^0, (b) - associated production of S-channel resonances, and (c) is the Deck effect.

Photoproduction of a mesonic state in the t-channel on the spin and isospin zero ($S = 0$ and $I = 0$) target coherently, i.e. when the target nucleus stays intact, is a powerful method to simplify significantly the PWA analysis.

The main final states to be studied are (see Fig. 5):

$$\gamma^{*}\ {}^4He \to \pi^0\eta\ {}^4He \ \to \ \gamma\gamma\gamma\gamma\ {}^4He \quad (1)$$

$$\gamma^{*}\ {}^4He \to \pi^0\eta'\ {}^4He \ \to \ \pi^+\pi^-\gamma\gamma\gamma\ {}^4He \quad (2)$$

$$\to \ \pi^+\pi^-\gamma\gamma\gamma\gamma\ {}^4He. \quad (3)$$

Decay modes of $\pi^0 \to \gamma\gamma$ and $\eta \to \gamma\gamma$ will be used to detect pions and etas. For the η' decay channels, $\eta' \to \rho^0\gamma(\pi^+\pi^-\gamma)$ and $\eta' \to \pi^+\pi^-\eta$ will be explored.

The resonant state in the $\pi^0\eta$ and $\pi^0\eta'$ channels will be reconstructed in the analysis of the decay angular distributions. The proposed reactions have several advantages for studying exotics:

- The final state $\pi^0\eta$ ($\pi^0\eta'$) has $I = 1$, $G = -1$, $C = +1$ and $J = (-1)^L$, where L is the angular momentum of the final state mesons. Hence a resonance in a P wave will be an exotic $I^GJ^{PC} = 1^-1^{-+}$

- Photoproduction of the $\pi^0\eta$ ($\pi^0\eta'$) system can proceed only via $C = -1$ exchanges. At small momentum transfer these are ρ^0 or ω exchanges, or Natural Parity Exchange (NPE) processes. This leads to a significan simplification of PWA

- No background from S-channel baryon resonance production

- The helicity of the produced state will be that of the incoming photon, $\lambda = \lambda_\gamma$, therefore production of $\pi^0\eta$ ($\pi^0\eta'$) in the S state is forbidden

The key feature of this experiment is that the recoiling helium nuclei stay intact. To ensure coherent production, the detection of helium nuclei, α-particles, in the final state is required. This requirement imposes constraints on the kinematics of the experiment and on the experimental setup.

In our energy domain, the mass range in the t-channel from 1.4 to 2 GeV will be covered at sufficiently low momentum transfer. In Fig. 7.a the distribution of the kinetic energy of the recoiling ^{4}He as a function of the mass of the produced state is shown. The lower edge of the distribution corresponds to the t_{min} at the highest available energy (i.e. 6 GeV). For the most interesting region of masses, 1.4 to 1.8 GeV, the recoiling nuclei, α-particles, will scatter mostly in the angular range from 20^o to 60^o with kinetic energies $E_{kin} \geq 0.007$ GeV (or momentum $p \geq 0.23$ GeV/c) (see Fig. 7.b).

Production rates in coherent scattering will depend on the ^4He form-factor, and therefore (taking also into account the t-dependence of the elementary cross section), the measurements must be carried out at a smaller momentum transfer, close to the minimum transferred momentum as possible. The recoiling α's in our kinematics will have only a *few* hundred MeV/c momentum and would not emerge from the liquid helium target. Even with pressurized gas targets, the threshold for detection of α's is $p > 0.28$ GeV/c (corresponding to transferred momenta of $|t| > 0.08$ (GeV/c)^2).

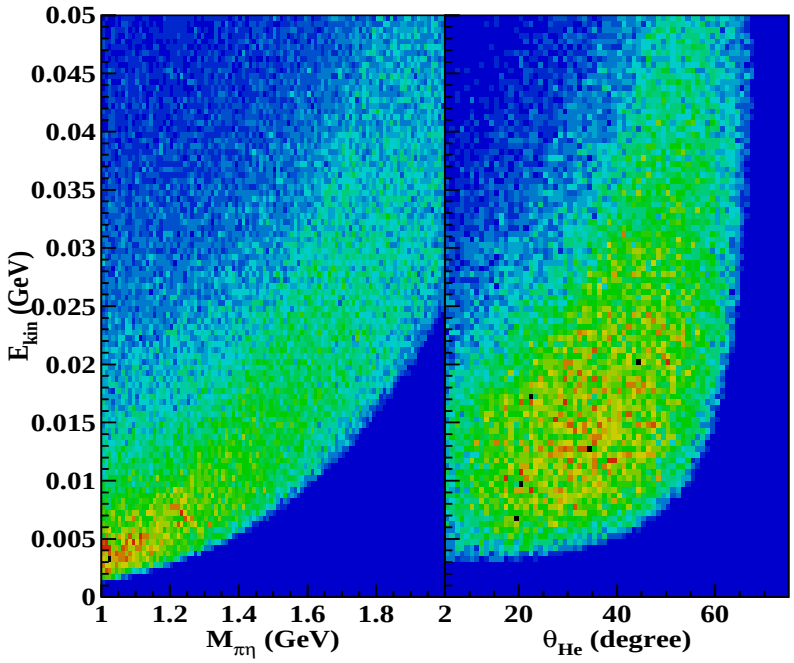

Figure 7: a) - the kinetic energy of ^{4}He nuclei as a function of the mass of the produced state in the t-channel. b) - the angular and momentum distribution of recoiling nuclei for the mass range 1.2 to 1.8 GeV.

Using a gas target with photon beams has two problems. First the conventional photon-tagging method is limited by the luminosity that is achievable with a reasonable accidental rate in the tagging system. Second, more relevant to these measurements, is the large beam size. The thickness of the target cell walls are proportional to the target diameter. At the same pressure, the larger the target diameter, the thicker the target cell walls must be, which presents more material in the path of the outgoing particles. This is important for detection of low energy α-particles.

For these reasons we have chosen to use electron scattering at very small angles. This is an attractive alternative to photoproduction. **Quasi-real photoproduction** is ideal for performing experiments on "thin" targets. The required luminosity can be achieved by increasing the primary beam intensity. A small-size (few hundred μm diameter), high-precision electron beam allows use of a small diameter target cell. Another advantage is that with a small size beam, the interaction point on the plane perpendicular to the direction of the beam will be better defined compared to a bremsstahlung photon beam. This is important for defining the production vertex in multi-photon final states.

4 PWA Formalism

Partial wave analysis is the key element in any meson spectroscopy experiment. The contributions of different spin and parity states, decaying into the same final state particles, are determined through a fit to the angular distribution of the decay products. The number of parameters in the fit, and therefore the required statistics, depends on the rank of the decay density matrix. The latter is defined by the number of spin and helicity states of the incoming and outgoing particles, and on the t-channel exchange mechanism.

In photoproduction (as in the case of pion beams) the mechanisms leading to natural parity and unnatural parity exchange (NPE and UPE) in the t-channel do not interfere. They contribute to different amplitudes with different angular dependences. In the case when the production mechanism is defined, this provides an additional constraint on the angular dependences of the amplitudes.

In the rest frame of the $\pi^0\eta$ ($\pi^0\eta'$) system, the Gottfried-Jackson frame (GJ), the differential cross section of $\pi^0\eta$ ($\pi^0\eta'$) photoproduction via t-channel exchange can be written as[3]:

$$\frac{d\sigma}{d\Omega} \;=\; |A_0 \;+\; A_-|^2 \;+\; |A_+|^2 \;, \tag{4}$$

where the helicity amplitudes of UPE are:

$$A_0 \;=\; \sum_{L=0}^{L_{max}} (2L+1)^{1/2} L_0 D^L_{00}(\Theta,\phi), \tag{5}$$

[3]Here and in the following we will follow the approach from Ref. [10].

$$A_- = \sum_{L=0}^{L_{max}} \sum_{\lambda=1}^{L} (2L+1)^{1/2} \sqrt{2} L_{\lambda -} Re(D^L_{\lambda 0}(\Theta, \phi)) \ , \tag{6}$$

and the amplitude for NPE is:

$$A_+ = \sum_{L=0}^{L_{max}} \sum_{\lambda=1}^{L} (2L+1)^{1/2} \sqrt{2} L_{\lambda +} Im(D^L_{\lambda 0}(\Theta, \phi)) \ . \tag{7}$$

Here L is the total angular momentum of the $\pi^0\eta$ ($\pi^0\eta'$) system and the sum goes up to the highest possible angular momentum of the produced pair in the given mass range. The second sums in Eq.(6) and Eq.(7) correspond to the possible helicity states of the pair, λ. L_0 and $L_{\lambda -}$ are the amplitudes for the production of $\pi^0\eta$ ($\pi^0\eta'$) with spin L via UPE, and $L_{\lambda +}$ the amplitude for the production via NPE. These amplitudes are parameters in the PWA. In each energy bin the angular distribution of the decay mesons will be analyzed to determine the production strength of a particular wave. The function $D^L_{\lambda 0}(\Theta, \phi)$ defines the angular distribution of the π (or η/η') in the GJ frame. Θ and ϕ are the polar and azimuthal angles of the meson in that frame.

We propose to perform PWA via investigation of the angular distribution of the π (or η/η') in the GJ frame using the formulas in Eqs.(5), (6), and (7). We expect, however, significant simplification of the expressions in Eqs.(5), (6), and (7) due to the following reasons:

1. At laboratory energies of the incoming particle $\geq$ 4 GeV, a successful description of different reactions with γ and π beams (see, for example, Refs. [45, 46, 47]) has been obtained taking into account the following trajectories:

   - P and P' with $I = 0,\ C = +1$,
   - nearly degenerate π ($I = 1,\ C = +1$) and b_1 ($I = 1,\ C = -1$),
   - nearly degenerate ρ ($I = 1,\ C = -1$) and a_2 ($I = 1,\ C = +1$),
   - nearly degenerate ω ($I = 0,\ C = -1$) and f_2 ($I = 0,\ C = +1$).

   From these trajectories, only the natural parity trajectory ω ($I = 0,\ C = -1$) can contribute to $\gamma\ ^4He \to (\pi\eta)\ ^4He$. Regge-cut terms violate parity of the t channel exchange, and contributions with unnatural parity can arise. At $E_L \geq 4$ GeV, a good description of reactions with γ and π beams has been achieved taking into account only cuts produced by Pomeron exchange (see, for example, Refs. [46, 47]). We have estimated the contributions of such cuts within the approach used in Refs. [46, 47]. It turned out that at $|t - t_{min}| \leq 0.1$ (GeV/c)^2, where in the proposed experiment the main number of events is expected, the contribution of the ωP cuts is suppressed in comparison with the contribution of ω exchange at least by a factor of 3-4. As contributions with natural and unnatural parity exchanges do not interfere with each other, we expect that in the

cross section the contribution of unnatural parity exchange will be suppressed by an order of magnitude relative to natural parity ω exchange, and in the cross section, only the contribution of A_+ will survive.

2. As the spin of ^4He is equal to 0, at $t = t_{min}$, λ should be the same as that of the initial photon, and in A_+, only the contribution with $\lambda = 1$ survives. When $|t - t_{min}|$ increases, helicity-flip amplitudes are switched on. Helicity amplitudes with $|\lambda| \geq 2$ are suppressed in comparison with the helicity amplitude with $\lambda = \lambda_\gamma$ by a factor proportional to (see e.g. [48])

$$\left(\frac{p_\perp}{GeV}\right)^n = \left(\frac{|t - t_{min}|^{1/2}}{GeV}\right)^n , \; n \geq 1 \tag{8}$$

and in the cross section, therefore, the contribution of the helicity-flip amplitudes will be suppressed in comparison with that of the helicity-non-flip amplitude by a factor proportional to $A_{sup} = \left(\frac{t-t_{min}}{GeV^2}\right)^n$, where $n \geq 1$. In the proposed experiment where $|t - t_{min}| \leq 0.1$ (GeV/c)^2, $A_{sup} < 0.1$.

Under the conditions (1) and (2) above, the differential cross section for the reaction $\gamma\ ^4He \to\ \pi^0\eta\ (\pi^0\eta'\ )^4He$ will reduce to:

$$\frac{d\sigma}{d\Omega} = |A_+|^2;\ A_+\ =\ \sum_{L=1}^{L_{max}} (2L+1)^{1/2}\sqrt{2}L_{1+}Im(D^L_{10}(\Theta,\phi))\ . \tag{9}$$

The function $D^L_{10}(\Theta,\phi)$ can be expressed through d-functions [30] as:

$$D^L_{10}(\Theta,\phi)\ =\ d^L_{10}(\Theta)e^{i\phi}, \tag{10}$$

and

$$Im(D^L_{10}(\Theta,\phi))\ =\ d^L_{10}(\Theta)\sin\phi. \tag{11}$$

Finally, under the conditions (1) and (2), the differential cross section for the production of interfering waves with L up to 3 will be:

$$\begin{aligned}\frac{d\sigma}{d\Omega}\ &=\ 3|P_{1+} + \sqrt{5}D_{1+}\cos\Theta \\ &+\ \frac{\sqrt{5}}{2}F_{1+}(5\cos^2\Theta - 1)|^2\sin^2\phi.\end{aligned} \tag{12}$$

The amplitudes P_{1+}, D_{1+}, and F_{1+} will be determined via analysis of the angular distribution of the produced mesons $\pi^0\eta$ $(\pi^0\eta'\ )$. The exotic state $J^{PC} = 1^{-+}$ is expected as a resonance in P_{1+}.

Let us note, that the $\sin^2\phi$ dependence of the cross section will be violated by the violation of each of the conditions (1) and (2). So, the ϕ dependence of the cross section will allow us to check the fulfillment of the above assumptions. Even if the assumptions do not hold as well as expected, the PWA can still be accomplished at the expense of more amplitudes in the sum of Eq.12. There is a well developed framework for the general PWA analysis in the CLAS Collaboration. It was used successfully in the analysis of the CLAS photoproduction data at 5.5 GeV (g6 experiment [13]).

5 Photoproduction Cross Sections

In addition to the exotic states $\pi_1(1400)$ and $\pi_1(1600)$ which we will look for in the channels $\pi\eta$ and $\pi\eta'$, in this range of masses one can expect significant contribution from the $a_2(1320)$, which has a large branching ratio to the $\pi\eta$ channel: $Br(a_2(1320) \to \pi\eta) = 0.145 \pm 0.012$, and is seen in the $\pi\eta'$ channel: $Br(a_2(1320) \to \pi\eta') = (5.3 \pm 0.9)10^{-3}$ [30] [4]. Here we present cross section estimates for π_1 and a_2^0 photoproduction. In this analysis it is expected that the a_2 will be used as the phase reference state.

5.1 Cross sections for the $\pi_1(1400)$ and $\pi_1(1600)$

The preferred mechanism for the coherent production of these states on ^4He is t-channel ω exchange, which has relevant quantum numbers $C = -1$, $I = 0$, $G = -1$, and a large coupling constant, $g_{\omega pp}$, corresponding to spin non-flip forward scattering on nucleons: $g_{\omega pp} = 8 - 14$ [44] and $g_{\omega pp} = 21$ [49].

The most uncertain ingredient here is the value of the coupling constant $\gamma\omega\pi_1$. This quantity could be found from the direct calculation of the $\pi_1 \to \gamma\omega$ transition in the flux-tube model, as was made for the radiative decay of the hybrid meson a_{1H} with $J^{PC} = 1^{-+}$, $I^G = 1^+$ to $\pi\gamma$ in Ref. [50]. However, in the flux-tube approach we have oscillations in the two-dimensional space transverse to the $q\bar{q}$ axis, which appear as transverse component in the quark wave functions for hybrids. If calculations are made in a non-relativistic approach, non-zero matrix elements can be obtained only in those cases when the electromagnetic transition operator between the quarks contains transverse component of quark momentum. This takes place for the electric dipole operator, which is responsible for $a_{1H} \to \pi\gamma$ [50]. In contrast with this, $\pi_1 \to \omega\gamma$ is a magnetic dipole or electric quadrupole transition, which contains transverse components of quark momentum in zero or second degree. For this reason non-relativistic calculations in the flux-tube approach give zero value for the $\pi_1 \to \omega\gamma$ amplitude.

[4] Another resonance which can contribute in this range of masses, taking into account its quantum numbers, is the $a_0(1450)$. It was seen in both the $\pi\eta$ and $\pi\eta'$ channels, however, there is no information on the corresponding branching ratios.

The coupling constant $\gamma\omega\pi_1$ can be found also in an indirect way by calculating the $\pi_1 \to \rho\omega$ amplitude with subsequent use of the vector meson dominance approach. In this case in the non-relativistic approach, we have again zero value for the $\pi_1 \to \gamma\omega$ amplitude. Indeed in the flux-tube approach, the $\pi_1 \to \gamma\omega$ amplitude is proportional to $\beta_\rho^2 - \beta_\omega^2$, where $\beta_\rho,\ \beta_\omega$ are the mean values of the quark momenta in the ρ and ω, which are close to each other. However, there are arguments, presented in Ref. [51], that suppression connected with the factor $\beta_\rho^2 - \beta_\omega^2$ may be overruled when the "ρ" is a γ, i.e. when the ρ is off the mass-shell. For the estimation of the possible value of transition matrix elements in such cases, Refs. [51, 52] present the reduced matrix elements that are obtained through dividing the calculated matrix elements by the dimensionless ratio $(\beta_\rho^2 - \beta_\omega^2)/(\beta_\rho^2 + \beta_\omega^2)$. These matrix elements appeared to be not small. For example, in Ref. [51], the following value is presented for the $\pi_1 \to \gamma\omega$ decay width:

$$\Gamma(\pi_1 \to \gamma\omega) = 180\ keV, \tag{13}$$

which is found from the reduced value of the $\pi_1 \to \gamma\omega$ amplitude.

A similar effect is found also for the $\pi_1 \to \pi\rho$ decay in Ref. [7]. This decay is forbidden in the non-relativistic flux-tube approach. However, by shrinking the π to a point-like current in Ref. [7], a non-zero value for the $\pi_1 \to \pi\rho$ width is obtained which is in agreement with the experimental observation [34].

In our estimations of the $\gamma(k)p(p_1) \to \pi_1(P)p(p_1)$ cross section, we will proceed from the vertices:

$$\omega(q)p(p_1)p(p_2):\ \ g_{\omega pp}\bar{U}(p_2)\gamma_\mu\omega^\mu U(p_1), \tag{14}$$

$$\gamma(k)\omega(q)\pi_1(P):\ \ g_{\pi_1\omega\gamma}[\pi_{1\mu}\omega_\nu F^{\mu\nu} - \frac{1}{m_{\pi_1}^2}\pi_{1\mu}P_\nu F^{\mu\nu}(\omega P)]. \tag{15}$$

Here in parentheses the momenta of the particles are presented, $F^{\mu\nu} = \varepsilon^\mu k^\nu - k^\mu\varepsilon^\nu$; $\varepsilon_\mu,\ \omega_\mu,\ \pi_{1\mu}$ are the polarization vectors of the $\gamma,\ \omega,\ \pi_1$, respectively. With the $\gamma\omega\pi_1$ vertex (see Eq.15), the width of the $\pi_1 \to \gamma\omega$ decay is equal to:

$$\Gamma(\pi_1 \to \gamma\omega) = \frac{g_{\pi_1\omega\gamma}^2}{6\pi}\frac{k^3}{m_{\pi_1}^2}(1 + \frac{k^2}{2m_\omega^2}). \tag{16}$$

Using for the $\pi_1 \to \gamma\omega$ decay width the value from Eq.(13), we find for the coupling constant $g_{\pi_1\omega\gamma} = 0.12$.

With the vertices from Eqs.(14,15), the π_1^0 photoproduction cross section on the proton is equal to:

$$\frac{d\sigma}{dt}(\gamma p \to \pi_1 p) = \frac{g_{\pi_1\omega\gamma}^2 g_{\omega pp}^2}{128\pi}\frac{S^{2(S_\omega-1)}}{(t - m_\omega^2)^2}390\mu b/GeV^2, \tag{17}$$

where all quantities are in GeV units. We have Reggeized this cross section using the commonly used procedure which consists in the following replacement [45]:

$$\frac{S^{S_\omega-1}}{t-m_\omega^2} \Rightarrow \left(\frac{s}{s_0}\right)^{\alpha_\omega(t)-1} \frac{\pi\alpha'_\omega}{sin(\pi\alpha_\omega(t))}\frac{1}{\Gamma(\alpha_\omega(t))}\frac{-1+e^{-i\pi\alpha_\omega(t))}}{2}, \tag{18}$$

$$\alpha_\omega(t) = 0.44 + \alpha'_\omega t,\ \alpha'_\omega = 0.9\ GeV^{-2}, s_0 = 1\ GeV^2. \tag{19}$$

5.2 Cross section for the $a_2^0(1320)$

The cross section for $a_2^0(1320)$ photoproduction has been estimated assuming that the main mechanism responsible for coherent production of $a_2^0(1320)$ on ^4He is t-channel ω exchange. Let us define the vertex $a_2\omega\gamma$ in the following way:

$$a_2(P)\omega(q)\gamma(k):\ eg_{a_2\omega\gamma}\frac{P^\nu P^\rho}{m_{a_2}^3}(\varepsilon_\mu k_\nu - \varepsilon_\nu k_\mu)\omega_\sigma q_\rho a^{\mu\sigma}. \tag{20}$$

Here in parentheses the momenta of the particles are presented, and ε_μ, ω_μ, $a_{\mu\sigma}$ are the polarization vectors of the γ, ω, a_2, respectively. With this vertex, the a_2^0 photoproduction cross section on the proton is equal to:

$$\frac{d\sigma}{dt}(\gamma p \to a_2^0 p) = \frac{\alpha}{256}g_{a_2\omega\gamma}^2 g_{\omega pp}^2 \frac{S^{2(S_\omega-1)}}{(t-m_\omega^2)^2} 390\mu b/GeV^2, \tag{21}$$

where all quantities are in GeV units. We have Reggeized this cross section using the replacement of Eq.(18).

The $g_{a_2\omega\gamma}$ coupling constant can be found from the experimental data for $\Gamma(a_2 \to \gamma\gamma)$ using the vector meson dominance approach [54]:

$$\Gamma(a_2 \to \gamma\gamma) = \frac{\pi}{5}\alpha^2 m_{a_2} g_{a_2\omega\gamma}^2 F_\omega^2, \tag{22}$$

where $\alpha = 1/137$, and F_ω is the $\omega\gamma$ coupling constant which is related to the $\omega \to e^+e^-$ width by

$$\Gamma(\omega \to e^+e^-) = \frac{4\pi\alpha^2}{3} m_\omega F_\omega^2. \tag{23}$$

Using experimental data:

$$\Gamma(a_2 \to \gamma\gamma) = 0.99\ keV\ [30], \tag{24}$$

$$\Gamma(\omega \to e^+e^-) = 0.59\ keV\ [30], \tag{25}$$

we have obtained

$$F_\omega = 0.058, \tag{26}$$

$$g_{a_2\omega\gamma} = 2.57\ . \tag{27}$$

Let us note that the width of the $a_2 \to \omega\gamma$ decay which corresponds to this value of $g_{a_2\omega\gamma}$ is

$$\Gamma(a_2 \to \omega\gamma) = \frac{\alpha}{3} g^2_{a_2\omega\gamma} \frac{k^3}{m^2_{a_2}} \frac{m^2_\omega + k^2}{m^2_{a_2}} \left(1 + \frac{k^2}{10 m^2_\omega}\right) = 341\ keV, \tag{28}$$

where k is the photon momentum in the a_2 rest frame. This width is compatible with $\Gamma(a_2 \to \pi\gamma) = 282\ keV$ [30].

In Fig. 8, the differential cross section, $d\sigma/dt$, for a_2^0 and $\pi_1(1400)$ photoproduction at 4.3 GeV (left panel) and for $\pi_1(1600)$ photoproduction at 5 GeV (right panel) are shown. These energy values are the average energy values for production of these mesons in our kinematics. Presented cross sections are calculated using a conservative value for $g_{\omega pp} = 14$. If use the value derived in Ref. [49], the cross sections will be a factor of 2 higher. In this calcuation the a_2^0 cross section at $t = t_{min}$ is 0.65 μb/GeV^2. For comparison, the measured cross section for $\gamma p \to a_2^+ n$ at $E_\gamma = 4.3\ GeV$ at $t = t_{min}$ is 10 $\mu b/GeV^2$ [55]. In Ref. [56], a good description of the experimental data for $\gamma p \to a_2^+ n$ has been obtained within a Regge-pole approach, where this reaction was described taking into account t-channel π exchange and the πP cut.

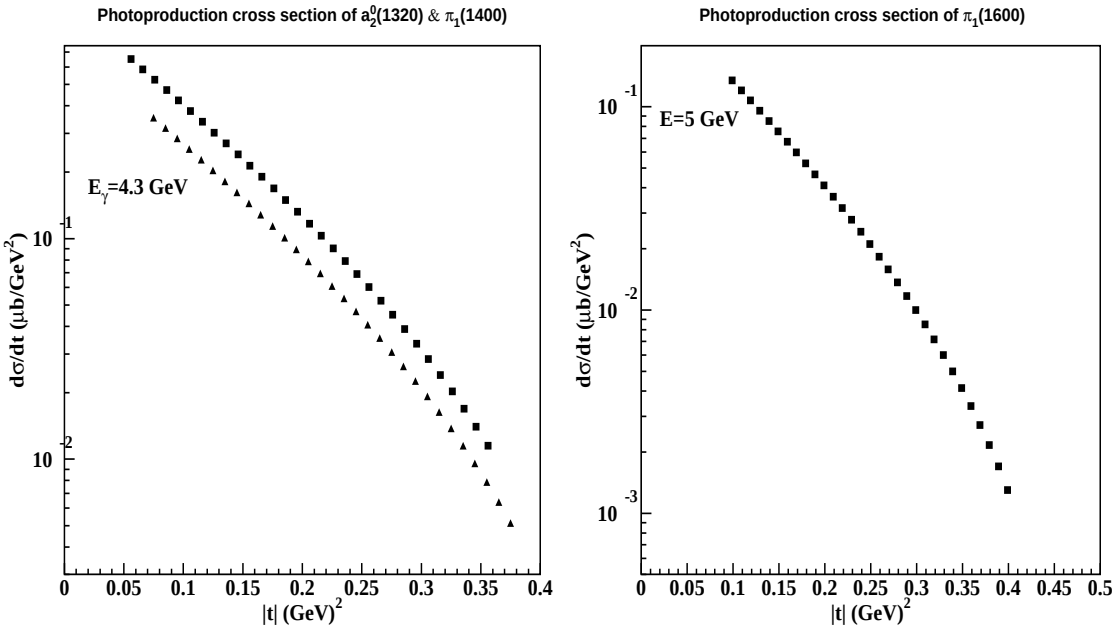

Figure 8: Photoproduction cross section for $a_2^0(1320)$ (boxes) and $\pi_1(1400)$ (triangles) at beam energy of $E = 4.3$ GeV, left graph. Cross section for $\pi_1(1600)$ at $E = 5$ GeV, right graph.

6 PWA sensitivity study

6.1 $\eta\pi^0$ system

To determine the sensitivity of an eventual partial wave analysis, a full GEANT based simulation including both the DVCS Inner Calorimeter (IC) and the Forward EM Calorimeter (EC) has been carried out for the reaction $\gamma\,^4He \rightarrow \eta\pi^0\,\,^4He \rightarrow \gamma\gamma\gamma\gamma\,^4He$. To simplify the study, only the two photon decay modes for the two pseudoscalar mesons were included. Assuming that the reaction contains only non-spin-flip amplitudes and that the meson helicity retains that of the photon, only pure $M = 1$ waves of $a_2(1320)$ and $\pi_1(1400)$ were generated in a t-channel process for photon energies between 4.6 and 5.6 GeV. The resonance parameters were $M = 1.318$ GeV/c^2, $\Gamma = 107$ MeV/c^2 for the 2^{++} state of $a_2(1320)$ and $M = 1.376$ GeV/c^2, $\Gamma = 300$ MeV/c^2 for the exotic 1^{-+} state of $\pi_1(1400)$. The t-slope used in the simulation was 4.0 (GeV/c^2)$^{-2}$ (as it is generally expected for π exchange).

The $2^{++}a_2(1320) \rightarrow \eta\pi^0$ decay angular distribution in the GJ frame (in a pure $M = 1$ wave) is of the form $sin^2\theta cos^2\theta$, while for the 1^{-+} state it is of the form $sin^2\theta$, as shown in Fig. 9. These two states show very distinct features in their decay distributions. The a_2 decay angular distribution goes to zero at $cos\theta = 0$ in the GJ frame, while the π_1 decay is at a maximum in the same place. By requiring exactly four photons detected by the IC and/or EC, making all possible two photon combinations, and requiring the reconstructed two photon invariant masses to fall into the $\eta\pi^0$ regions as shown in Fig. 10, the $\eta\pi^0$ events could be reconstructed.

The uncertainty of reconstruction of the angles of the η and π^0 and geometrical acceptance modifications, lead to the deviation from zero in the a_2 angular distribution (Fig. 11). Comparing the deviation from zero at $cos\theta = 0$ of the $\eta\pi^0$ decay in the GJ frame offers a very conservative way to estimate the minimum number of $\pi_1(1400)$ needed to identify the exotic waves from the a_2 background events. From our estimated cross sections, we determine that around 40 k a_2 events can be reconstructed from the $\eta\pi^0$ channel. This is used as guidance for the sensitivity of the $\eta\pi^0$ PWA study through its decay angular distributions. If 9 k $\pi_1(1400)$ are produced in the $\eta\pi \rightarrow 4\gamma$ channel, the decay angular distribution will represent two standard deviations from zero at $cos\theta = 0$. We need to point out that this simulation does not include the interference between the $a_2(1320)$ and the $\pi_1(1400)$.

Brookhaven's E852 results on the $\pi_1(1400) \rightarrow \eta\pi^-$ were dominated by the $a_2(1320)$ signal, while the exotic signal comprises less than 4% of the total intensity [57]. The more important evidence for the exotic meson lies with the phase difference motion of the D_+ and P_+ waves. As discussed earlier, the photoproduction rate of the $\pi_1(1400)$ may be much higher than in pion production, and it is possible that by studying the angular distributions of the $\eta\pi$ system alone, the exotic waves could be extracted. The forward-background asymmetry from E852 $\eta\pi^-$ data is shown in Fig. 12. The asymmetry in the neighborhood of the $\pi_1(1400)$ due to the interference with the

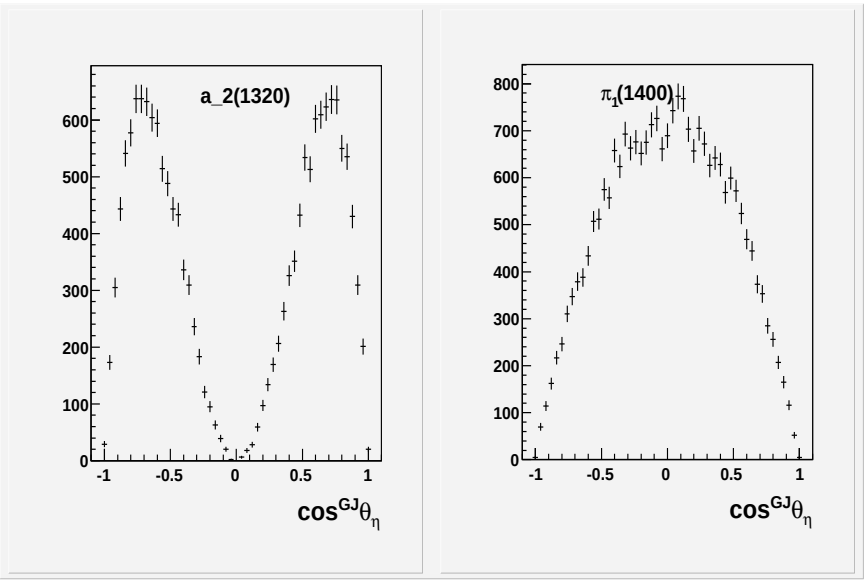

Figure 9: Generated angular distributions of the $\eta\pi^0$ decays of the $a_2(1320)$ (left) and $\pi_1(1400)$ (right) decays in the GJ frame (η is the analyzer particle) with only $M = 1$ components.

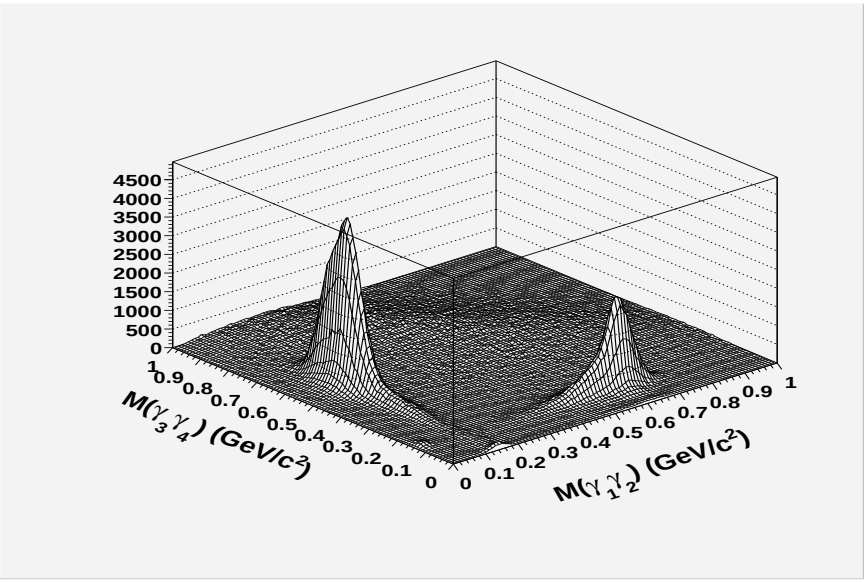

Figure 10: Accepted $\eta\pi^0 \to 4\gamma$ events from $a_2(1320)$ and $\pi_1(1400)$ decays.

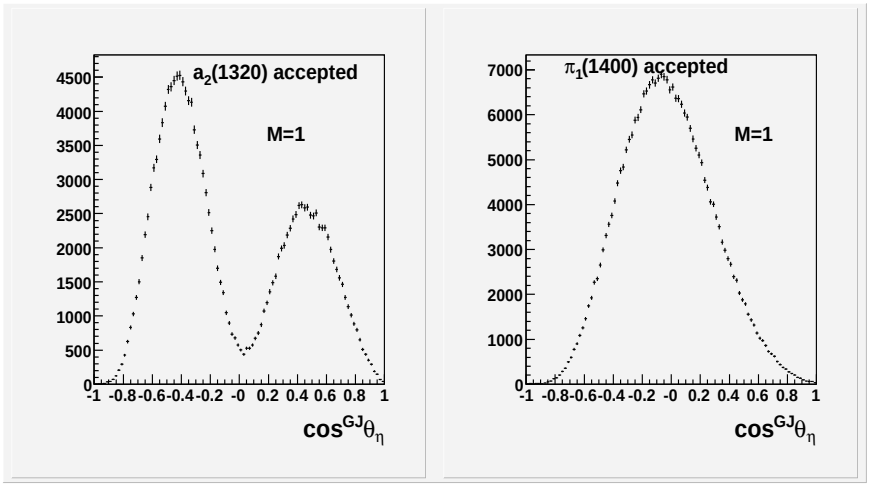

Figure 11: Accepted angular distributions of the $\eta\pi^0$ decays of the $a_2(1320)$ (left) and $\pi_1(1400)$ (right) decays in the GJ frame with only $M = 1$ components.

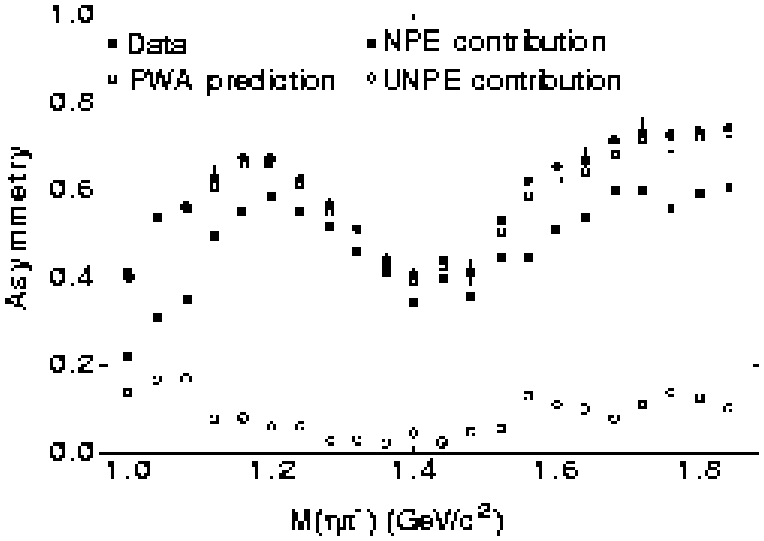

Figure 12: $\eta\pi^-$ asymmetry as a function of mass.

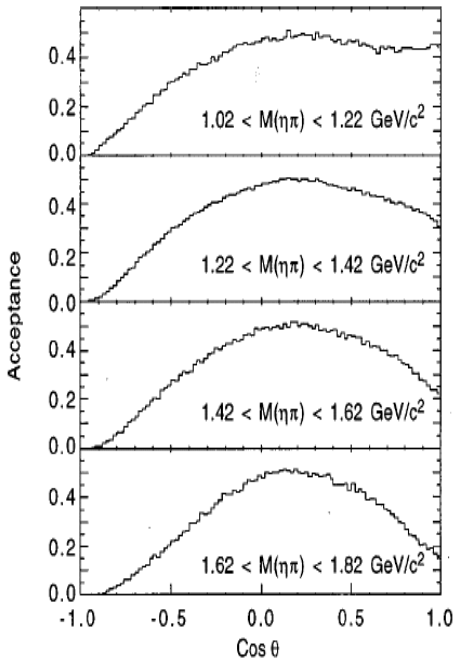

Figure 13: The E852 acceptance as a function of cos^{θ} in the GJ frame of the $\eta\pi^-$ system [57], with η as the analyzer.

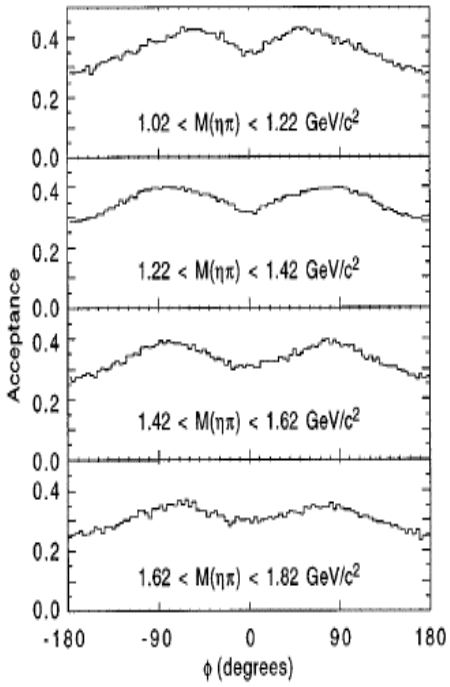

Figure 14: The E852 acceptance as a function of ϕ in the GJ frame of the $\eta\pi^-$ system [57], with η as the analyzer.

$a_2(1320)$ is about 40%. In the 2-pseudoscalar system ($\eta\pi$), any asymmetry must come from an odd-even wave interference. As a result, after a partial wave analysis, the number of events in the exotic P_+ wave is approximately 4% of the $a_2(1320)$ events. A systematic error in the acceptance correction could generate a false asymmetry, and of course the potential for systematic errors increases when the acceptance is a rapidly varying function of $cos\theta_{GJ}$. The E852 acceptance in Gottfried-Jackson $cos\theta$ is shown in Fig. 13. It is clear that the acceptance itself suffers from a significant forward-backward asymmetry, with no acceptance in the backward direction.

To estimate the effect of the uncertainty in the acceptance, the decay angular distributions for the $a_2(1320)$ were corrected using a second acceptance obtained from a simulation that does not include any angular dependence (i.e., the decay is isotropic). In Fig. 15 (right), it is clear that without a perfect understanding of the CLAS detectors and acceptance, it is possible to generate a forward-backward asymmetry artificially. This asymmetry is studied as a function of $\eta\pi^0$ invariant mass (Fig. 15), and is in the order of 10%. This would lead to the systematic error of the exotic signals to be 1% of the $a_2(1320)$, well below the expected $\pi_1(1400)$

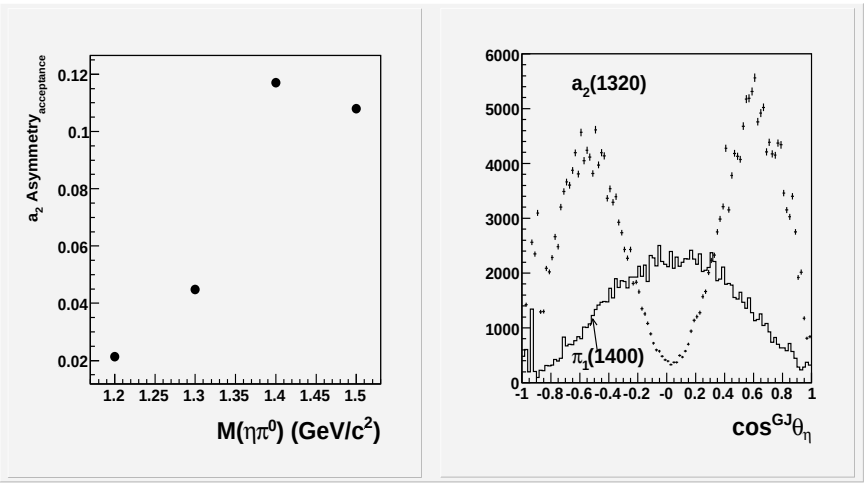

Figure 15: Left: The artificial asymmetry created by the acceptance uncertainties for $a_2(1320)$ events as a function of $\eta\pi^0$ invariant mass; Right: Acceptance corrected angular distributions with the total accepted $a_2(1320)$ events weighted to be 40 k, and the total number of $\pi_1(1400)$ 28 k.

signal. When analyzing the real data, this systematic error can still be minimized by using the experimental cross sections as an input to the simulations to obtain a better determination of the acceptance. Taking the 10% as a systematic error in the measurement of the forward-backward asymmetry, an observed 40% asymmetry in the real data would have meant a 3-5% exotic signal of the $\pi_1(1400)$ compared to the $a_2(1400)$ (Fig. 16).

The validity of the above discussions relies on two assumptions. The first is the suppression of spin-flip amplitudes which would justify ignoring the waves for $M = 2$. The existence of $M \neq 1$ waves can be investigated from both the $cos\theta$ distributions at the most forward and backward angles ($\sim (3cos^2\theta - 1)^2$ with $M = 0$ for 2^{++}) and the $sin^2\phi$ distributions as discussed in Section 5. Even if a full partial wave analysis is needed, the $\sim$ 50 k a_2 and $\sim$ 36 k $\pi_1(1400)$ events offers similar statistics as the E852 published data [57]. Compared with the acceptance of the E852 data (Fig. 13, 14), the CLAS acceptance of the $\eta\pi^0$ events using the Inner Calorimeter and the Forward Calorimeter (see Section 9) are similar if not better, which makes a full partial wave analysis realistic.

The second assumption, that there is no interference between the $a_2(1320)$ and the $\pi_1(1400)$, is only used as the most conservative estimate for the needed statistics. In fact, the interference effect only makes it easier to identify the exotic wave, as was demonstrated by the E852 results, where the exotic signal is more prominent in the phase motion between the a_2 and $\pi_1(1400)$ than in the intensity distribution ([57]).

To summarize, assuming only the non-spin-flip amplitudes survive, the analysis of

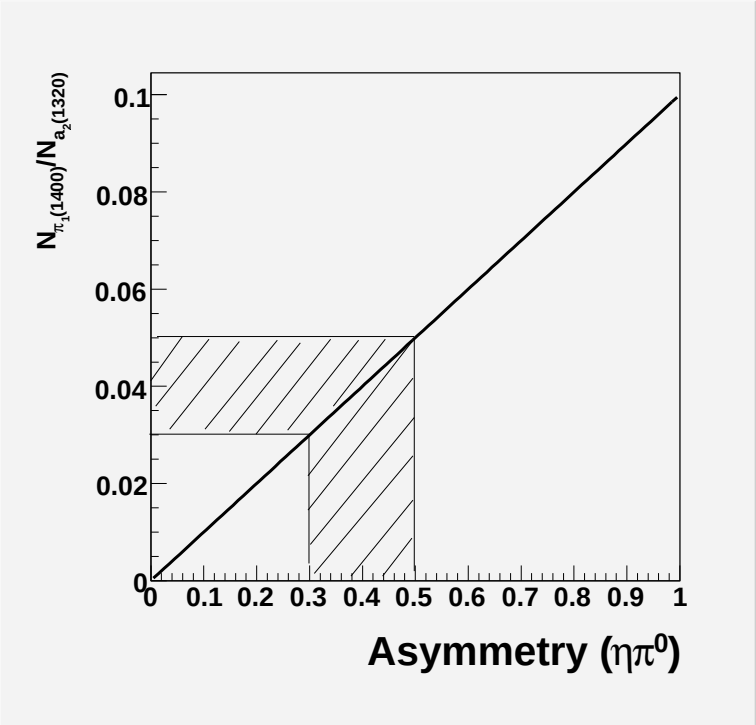

Figure 16: $\pi_1(1400)/a_2(1320)$ ratio as a function of the observed forward-backward asymmetry for the $\eta\pi^0$ system in the GJ frame. The shaded region indicates the expected systematic error.

the decay angular distributions of the $\eta\pi^0$ events in the coherent quasireal photoproduction on a ^4He target will be sufficient to extract exotic signals from the expected, dominant, $a_2(1320)$ background. Based on the GEANT simulations, about 9 k reconstructed $\pi_1(1400)$ events are required to separate the a_2 and $\pi_1(1400)$ signals at the two sigma level well below the 36 k events that are expected by our model predictions. If this model turned out to be wrong, the expected statistics will still be sufficient to conduct a full partial wave analysis comparable with the earlier experiments (i.e., E852).

6.2 $\eta'\pi^-$ system

In the $\eta'\pi^-$ system, the situation is much different. While in $\eta\pi$ the exotic state is only 4% of the data, in the $\eta'\pi$ system, the exotic wave *dominates* the data, as seen from the PWA results from E852 (see Fig. 4). In fact, the exotic $\pi_1(1600)$ may be seen directly in the effective mass plot (see Fig. 17). In this case, observation of the exotic state does not rely on the amplifying effect of the interference, and hence an asymmetry, but rather the J of the state is determined directly by the angular distribution of the 2 pseudoscalars, and therefore, any introduced systematic

uncertainties in the acceptance *do not* generate exotic signals.

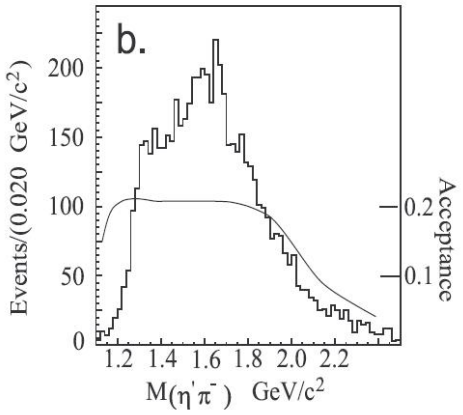

Figure 17: $\eta'\pi^-$ effective mass from E852.

7 Detector Configuration

For reconstruction of neutral mesons via their decays to $\pi^0\eta$ and $\pi^0\eta'$ final states in the reactions presented in Eqs.(1), (2), and (3), the following detector requirements are needed:

1. large acceptance for photon detection

2. detection of low energy ($P > 0.25$ GeV/c) recoiling α-particles

3. detection of the scattered electrons at small angles[5], $\theta_{e'} \to 0^o$

We will run the experiment in a similar detector configuration to that used for the BoNuS [58] and the e1-DVCS [59] experiments: the standard CLAS detector package with the DVCS solenoid, DVCS inner calorimeter (IC), BoNuS RTPC, and a 20 cm long gas target, see Fig. 18. The required beam energy is 5.5 to 6 GeV with a maximum intensity of 400 nA. The DVCS inner calorimeter will be positioned 55 cm downstream of the target center. The BoNuS target will be filled with ^4He gas at 7 atm pressure. The DVCS superconducting solenoid will provide longitudinal field along the beam line, and will be used for the tracking in the BoNuS RTPC and will work as a magnetic shield from the Moller electrons.

7.1 Photon detection

In 2005, the CLAS-DVCS experiment demonstrated excellent performance of a 424 channel $PbWO_4$ crystal calorimeter (IC). The IC was an important addition to the CLAS detector package for photon detection in the forward region. The calorimeter was successfully commissioned and calibrated in energy [60] and time [61], and now is used in the analysis of photon, π^0, and η electroproduction reactions.

In the proposed experiment, the IC will be used as a trigger device. For the DVCS run, the IC trigger was used only for calibration data taking. It was based on the multiplicity of hits in the whole calorimeter. Due to the common threshold for each 16 channel group, and the simple selection scheme employed, it was not very efficient and did not have a well defined energy threshold. Two improvements will be implemented to the trigger system for future use: individual channel control and a flexible logic organizer to make fast clustering. Both improvements are planned for the next DVCS experiment and will be implemented here.

[5]Detection of scattered electrons is not an absolute necessity. The physics analysis can be done without detection of the scattered electrons. Their kinematics can be deduced from the fully detected hadronic final states (see below). However, in many cases, it will help in the detector calibration and for the systematic studies.

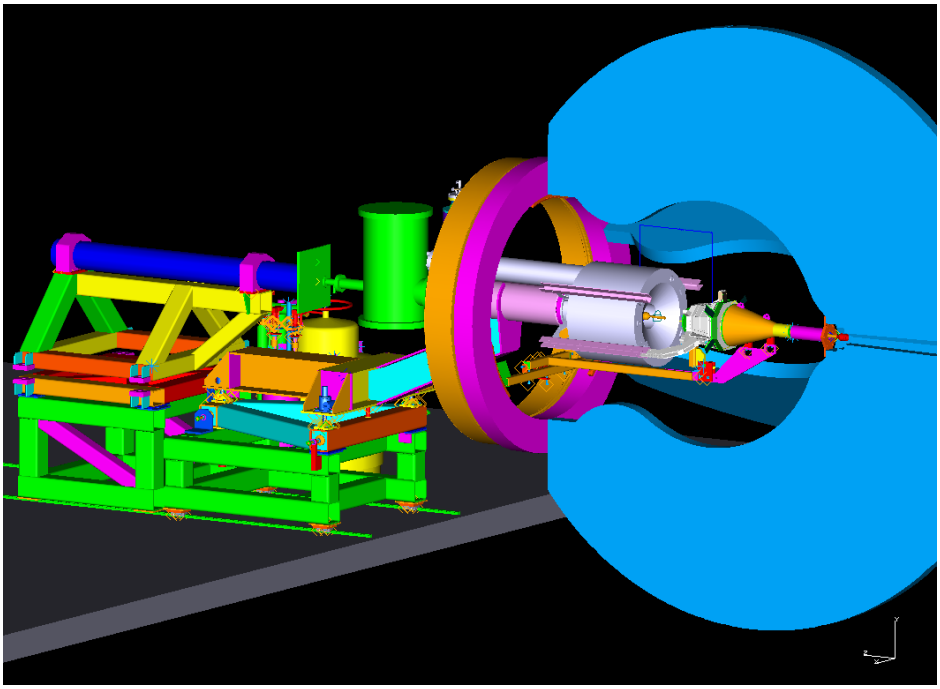

Figure 18: Proposed configuration for the CLAS detector.

7.2 Detection of low energy α-particles

To detect low energy recoiling ^{4}He nuclei we will use the Radial Time Projection Chamber (RTPC) from the BoNuS experiment. The BoNuS RTPC allows measurement of a track segment and the energy loss of a charged particle. Gas Electron Multipliers (GEMs) are used to collect signals from the RTPC. The same device, after replacing the deuterium gas with helium, will be used in our experiment. The threshold for ^{4}He detection will be 0.28 GeV/c. Particle identification will not be a problem since energy loss of a low energy ^{4}He nucleus will be significantly higher than for protons, deuterons, ^{3}H, and ^{3}He, see Fig. 19.

The data obtained during the BoNuS experiment are still in the calibration stage, however successful operation of the detector is already evident. In Fig. 20 the vertex distribution of a particle detected in CLAS vs. the vertex of a particle detected in the RTPC in the same event is shown. A clear correlation is seen. The Z-vertex resolution is $\sim$ 1 cm.

One of the issues during the BoNuS experiment was low event rate ($\sim$ 0.5 kHz). Currently work is in progress to improve the RTPC readout rate. Using the standard readout controller for the ALICE TPC front end cards, it is expected to reach a readout rate at least 1 kHz. Further discussions are presented in Section 11.

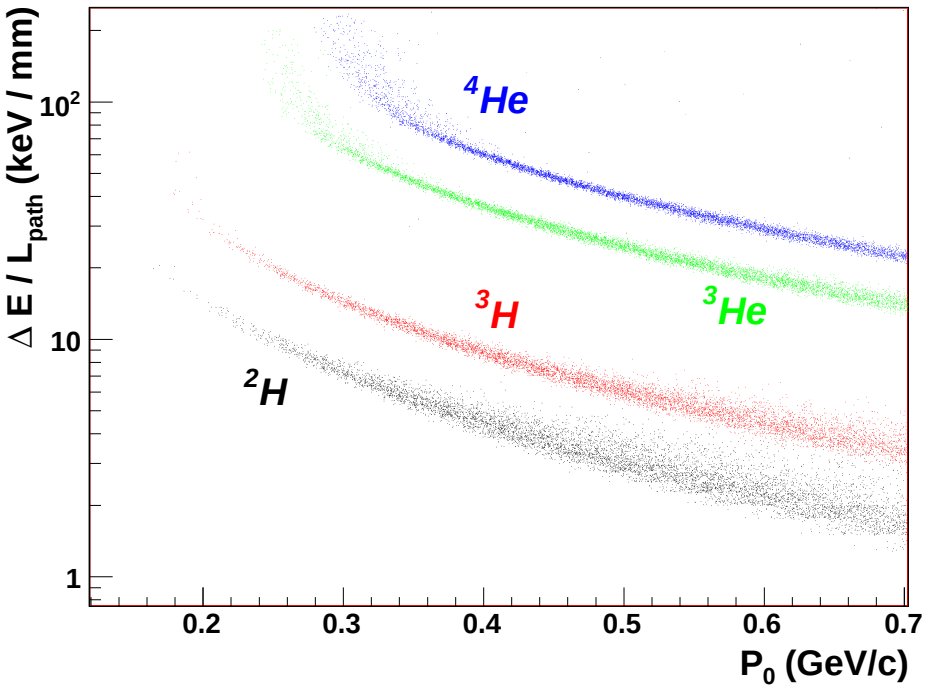

Figure 19: Energy loss as a function of momentum for deuterons, ^{3}H, ^{3}He, and ^{4}He from GEANT4 simulations of the RTPC.

7.3 Forward photon tagger

Finally, a new electron detector at small angles, $< 0.5^o$, will be built to tag electrons that interacted in the target. Currently we are proposing to build a simple magnetic spectrometer, based on the dipole magnet located in the downstream alcove in Hall B (the old pair spectrometer dipole). As a detector, a scintillating fiber array with multi-anode PMTs as readout will be used.

The total amount of material in the beam line before the spectrometer will be about 10^{-3} r.l., 20% of which is the target material. While it will not be possible to use this device directly in the trigger, it still will be useful to have that information in the data stream for the analysis. Low intensity runs will allow direct tagging of scattered electrons for calibration purposes.

It is important to point out that such a device will be extremely important for conducting quasi-real photoproduction experiments at higher energies, $E > 7$ GeV, where the present CLAS tagging system cannot reach.

7.4 Trigger setup

The main trigger for the CLAS DAQ will be a neutral trigger. In the three main final states there are 3 or 4 photons. From kinematics of the reactions of Eqs.(1), (2), and (3), there are almost always photons in the IC with energy above 0.5 GeV and a photon in one of the CLAS forward electromagnetic calorimeter modules (EC). Events with no photons in the IC always have photons in two different EC modules.

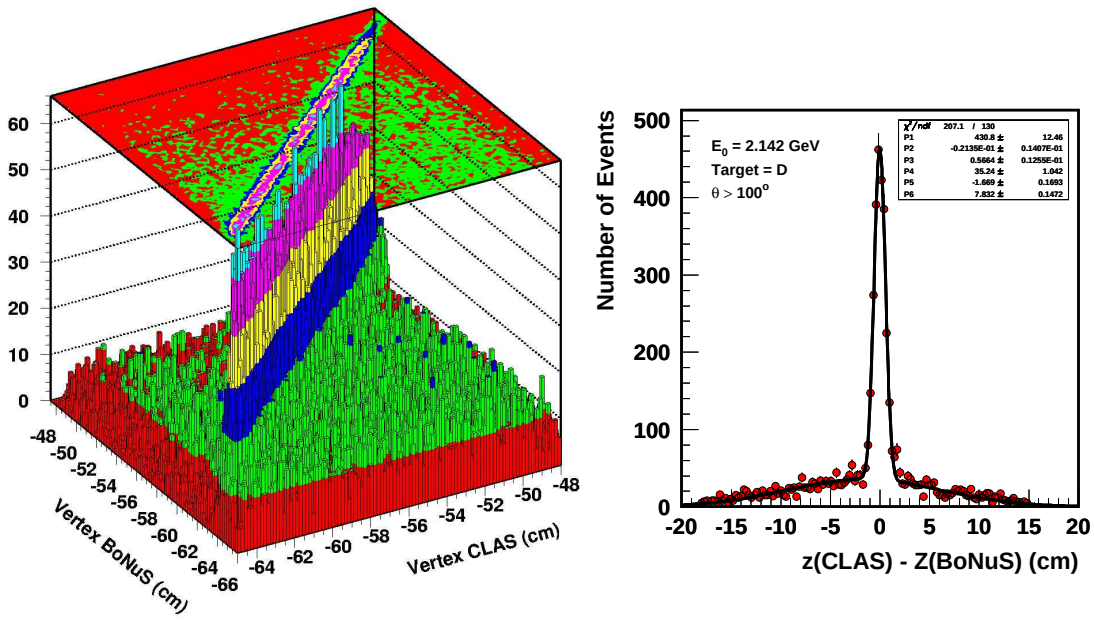

Figure 20: Correlation between the electron vertex as measured by the CLAS detector and the recoil proton vertex as measured by the BoNuS RTPC. The data were taken by scattering 2.1 GeV electrons off a deuterium target.

Considering these statements, our proposal for the trigger will be:

1. $EC_i \times IC(> 0.5GeV); i = 1, 6$
2. $EC_i \times EC_j; i, j = 1, 6$ and $i \neq j$

For both triggers, the threshold in the EC will be > 0.07 GeV energy deposition (corresponding to about 0.2 GeV photons). Trigger (2), EC only, is one of the standard CLAS trigger settings. Trigger (1) has not been used before, but, as was mentioned above, the IC alone trigger setting was used during the DVCS run for IC calibration runs. Using these runs and the DVCS production runs, an estimate on trigger rates was performed. It was found that trigger (2) in the CLAS-DVCS configuration will be $< 10\%$ of trigger (1). So the main trigger will be an $EC \times IC$ coincidence. Studies with DVCS data showed that at the luminosity of $L_C = 1.5 \times 10^{34}\ cm^{-2}sec^{-1}$ (luminosity of the calibration runs), the rate in trigger (1), using the same trigger setup as was used in the DVCS IC calibration, will be $\sim$ 11 kHz. With an improved, flexible trigger system in the IC, this rate can be lowered, without significantly affecting the physics data, to $\sim$ 5.5 kHz. For details of the trigger rate studies see Section 12.

Taking into account the limitation of $\sim$ 1 kHz on the DAQ rate imposed by the RTPC readout system, the limit on the luminosity will be $L = 3 \times 10^{33} cm^{-2}sec^{-1}$. The required beam current for this luminosity to run on a 20 cm long, 7 atm ^4He gas target will be $\sim$ 130 nA.

8 CLAS Performance

Various CLAS experiments have run with a configuration similar in part to the configuration required for this experiment. In this section, analyses of electroproduction and photoproduction experiments are presented with emphasis on quasi-real photoproduction of hadronic events in the electron scattering experiments and on the coherent photoproduction of mesonic final states.

8.1 Quasi-real photoproduction with e1-6 data

To show how well CLAS can handle multi-particle, and particularly multi-photon, final states, we analyzed data from the CLAS e1-6 electroproduction experiment at 6 GeV. The goal of this analysis was to identify the reactions:

$$\begin{aligned} ep &\rightarrow (e)p\pi^0\pi^0 \\ ep &\rightarrow (e)p\pi^0\eta, \end{aligned} \tag{29}$$

similar to what we are proposing for the coherent production on ^{4}He, without detecting the forward-going electron.

The main focus of the e1-6 experiment was the measurement of electron-proton scattering in the deep inelastic scattering region. Data were acquired using a "single electron" trigger. The CLAS Level 1 trigger was created by a coincidence of the forward calorimeter and the Cherenkov counter in the same sector.

Due to the "rejection" inefficiency of the Level 1 trigger, in addition to the real electron events (that account for $\sim 10\%$ of the trigger rate), coincidences from "non-electron" events were recorded as well. These are hadronic events produced mostly by "0" degree scattered electrons. For the analysis of the reactions in Eq.(29), we select events from "non-electron triggers" (events that did not have a reconstructed negative track) with at least one fitted positive track, and four neutral hits in the forward calorimeter:

$$ep \rightarrow p\gamma\gamma\gamma\gamma X. \tag{30}$$

In Fig. 21 the missing momentum vs. missing mass squared (M_X^2) is shown on the right panel for the selected sample. The M_X^2 distribution is consistent with 0 at low missing momentum. In addition, the distribution of the perpendicular component of the missing momentum peaks around zero, see the left panel of Fig. 21. These facts suggest that the missing particle is an electron with its momentum vector pointing in the direction of the beam (electron scattered at $\sim 0^o$). Therefore, applying cuts $-0.1 < MM^2 < 0.1$ GeV^2, and $\sqrt{(PX_x/PX)^2 + (PX_y/PX)^2} < 0.1$, we select the reaction:

$$ep \rightarrow p\gamma\gamma\gamma\gamma(e), \tag{31}$$

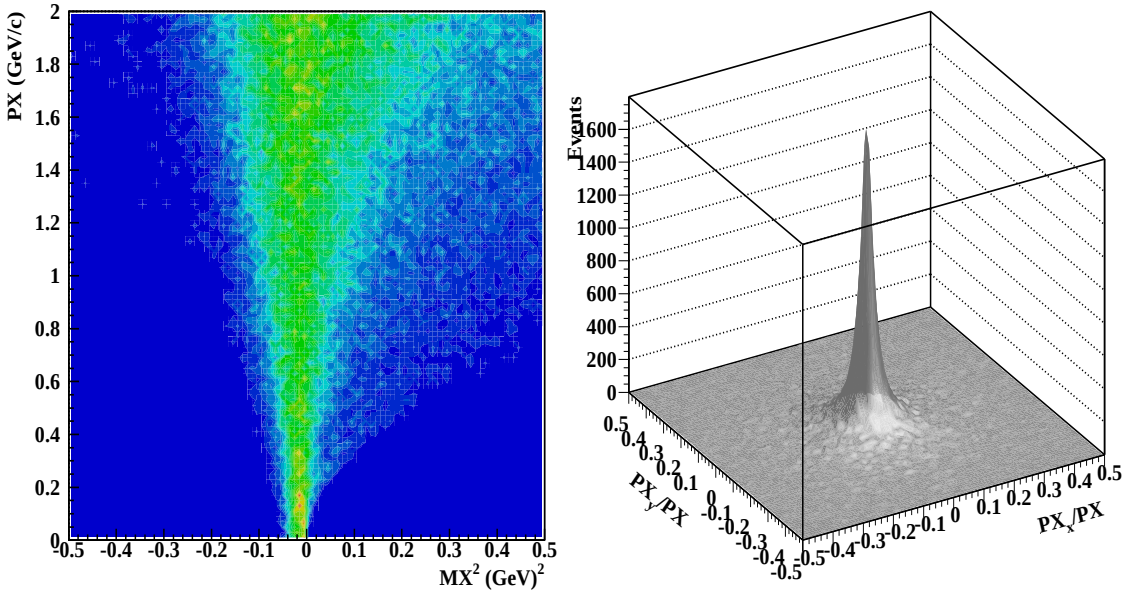

Figure 21: On the left - the distribution of the missing energy vs. missing mass squared in the reaction of Eq.(30). On the right - component of the missing momentum perpendicular to the direction of the beam, normalized to the absolute value of the missing momentum.

i.e. quasi-real photoproduction of the 4γ final state with a bremsstrahlung photon beam.

To select $\pi^0\pi^0$ and $\pi^0\eta$ final states, all possible combinations of two photons have been studied. In Fig. 22, the invariant mass of one pair of photons against the invariant mass of the other pair is plotted (graph on the left). One clearly sees $\pi^0\pi^0$ and $\pi^0\eta$ final states. The cuts on the invariant masses of two photons used for identification of π^0 and η are $0.1 < M_{\gamma\gamma} < 0.18$ GeV and $0.5 < M_{\gamma\gamma} < 0.62$, respectively.

After identifying the reactions $\gamma p \to p\pi^0\pi^0$ and $\gamma p \to p\pi^0\eta$, the invariant mass distributions for $\pi^0\pi^0$ and $\pi^0\eta$ are studied. The invariant mass distribution of the two π^0's is shown in Fig. 23.a. As one expects, $f_0(980)$ and $f_2(1270)$ are clearly seen. The invariant mass of the $\pi^0\eta$ system is presented in Fig. 23.b. There is a peak around 1 GeV where the $a_o(980)$ is expected, and a shoulder on the falling edge around 1.3 GeV, where the $a_2(1320)$ meson should be.

This analysis, although with data taken as a byproduct and not in an efficient way, clearly show the excellent performance of the CLAS detector in the reconstruction and identification of multi-photon final states in quasi-real photoproduction using a 6 GeV electron beam.

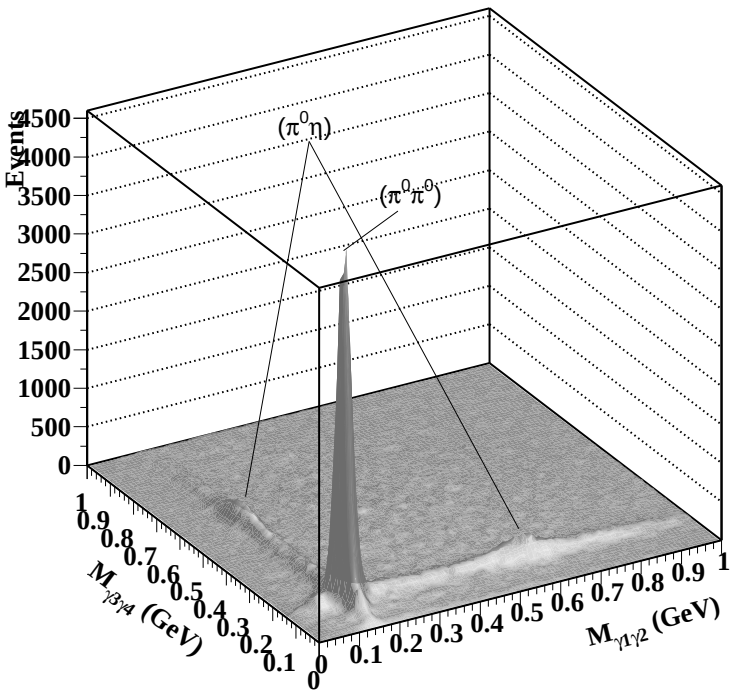

Figure 22: The invariant mass of two photons vs. the invariant mass of other two in the reaction $ep \to p\gamma\gamma\gamma\gamma(e)$.

8.2 Quasi-real photoproduction with the e1-DVCS data

We have also studied reactions in Eq. (29) on the e1-DVCS data [59]. In the e1-DVCS case, a new detector was added, a new $PbWO_4$ calorimeter (IC - inner calorimeter) in the forward direction [2]. The DVCS setup is very similar to the setup we plan to use in this experiment. Since DVCS just recently ran, these data are still being analyzed and their calibration is still preliminary.

We use events with a observed proton but with no scattered electron observed (the electron escapes detection through the forward acceptance "hole"). These events are then close to quasi-real photoproduction (very low Q^2 events). To select multi-photon final states, we look at signals in the IC and the EC (EM forward CLAS calorimeter). Clusters in the IC detector were selected if:

- Number of crystals in a cluster > 3
- Energy MAX Crystal/Total Energy > 0.4
- Energy in cluster > 0.3 GeV
- A fiducial geometric cut such that the centers of clusters (xc,yc) in the x,y plane were 5 cm $< \sqrt{xc^2 + yc^2} <$ 12 cm

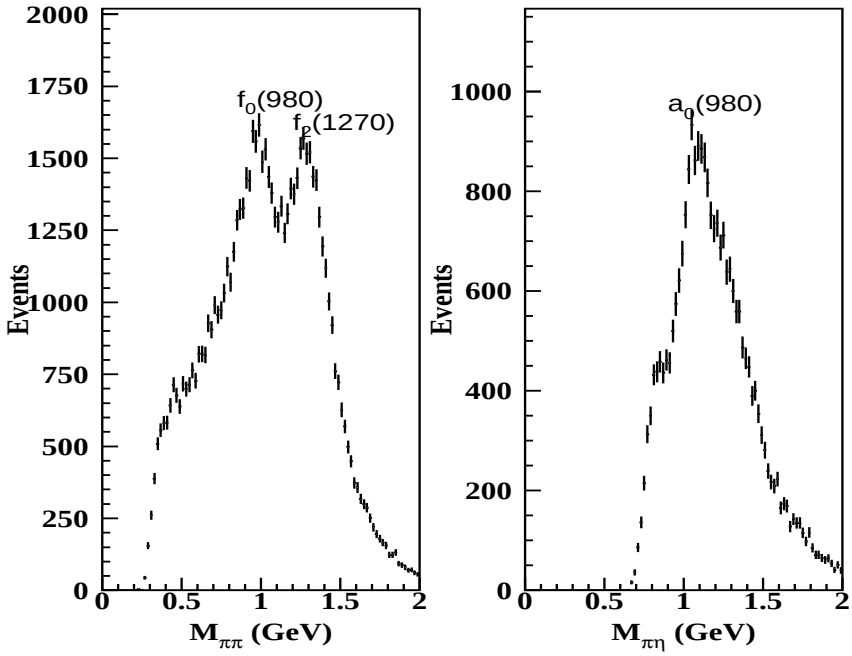

Figure 23: Invariant mass distributions for $\pi^0\pi^0$ (left) and $\pi^0\eta$ (right) events in the reactions $ep \to p\pi^0\pi^0(e)$ and $ep \to p\pi^0\eta(e)$, respectively.

All neutral particles with energies greater than 0.2 GeV were taken as photons from the EC calorimeter data. An energy correction was applied to the EC energies to match the observed π^0 mass with the PDG value [30]. Cuts on the missing mass and the missing momenta of events with only four photons and a proton were applied in a similar way to the e1-6 analysis.

Fig. 24 shows all possible combinations of invariant two-photon masses for events with only four photons. Many $\pi^0\pi^0$ events are seen and some small number of $\pi^0\eta$s. Fig. 25 shows the $\pi^0\pi^0$ and $\pi^0\eta$ invariant masses. The expected resonances are observed very close to the expected masses. This very preliminary analysis shows that it is possible to study multi-neutral, quasi-real photoproduction events in the e1-DVCS configuration. We plan to maximize the efficiency for the $\pi^0\eta$ modifying the IC to target distance to increase η detection efficiency.

8.3 Coherent photoproduction on deuterium

As an example of a coherent production process, the reactions $\gamma d \to K^+K^-d$ and $\gamma d \to \pi^+\pi^-\pi^0 d$ will be discussed. Although these are not the same final states as given earlier in this proposal, it is useful to examine some of the methods of analysis that will be applied in the proposed reaction. The deuterium data was chosen because

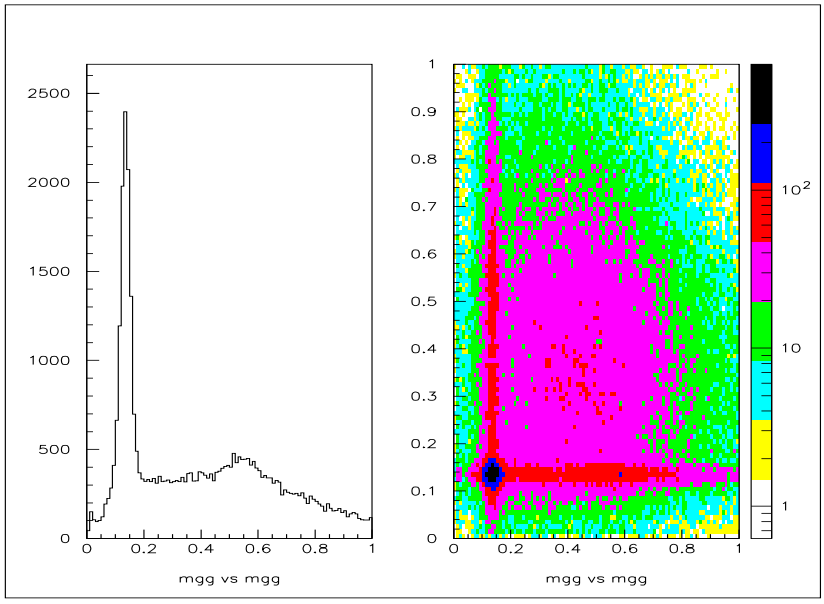

Figure 24: Four photons events from e1-DVCS: mass of two photons when the other two photons yield a pion, and a scatter plot of all possible two-photon versus two-photon mass combinations.

it has already been studied in depth at CLAS [62]. The data analysis is from the g10 experiment, using photons of up to 3.6 GeV on a deuterium target.

8.3.1 K^+K^- final state

The primary interest in this reaction is to study the ϕ resonance at 1019 MeV. However, the non-resonant background is also interesting. In Fig. 26, a plot of the missing mass for the $\gamma d \rightarrow dK^+X$ reaction is shown at the top, showing the K^- peak, and the invariant mass of the K^+K^- pair is shown at the bottom. Here, the 4-vector for the K^- is deduced from the missing momentum. The ϕ resonance is clearly seen in the $M(K^+K^-)$ spectrum. Angular distributions from the ϕ peak and from the non-resonance regions above and below the ϕ peak will be examined separately below. For the ϕ peak, we expect to see evidence of helicity conservation from the initial to the final state (also called s-channel helicity conservation in the literature), since the ϕ has the same quantum numbers as the incident photon and because the nearly pure $s\bar{s}$ nature of the ϕ implies that Pomeron exchange is dominant. It is not clear that the non-resonant background will necessarily show s-channel helicity conservation, and so we look to the data for evidence.

In the case of coherent scattering from ^4He, the target spin is zero and so the helicity of the photon will be passed on to the final state. In the case of coherent scattering from deuterium at small $|t|$, it is possible that s-channel helicity conservation could be dominant. To examine this possibility, first choose the quantization

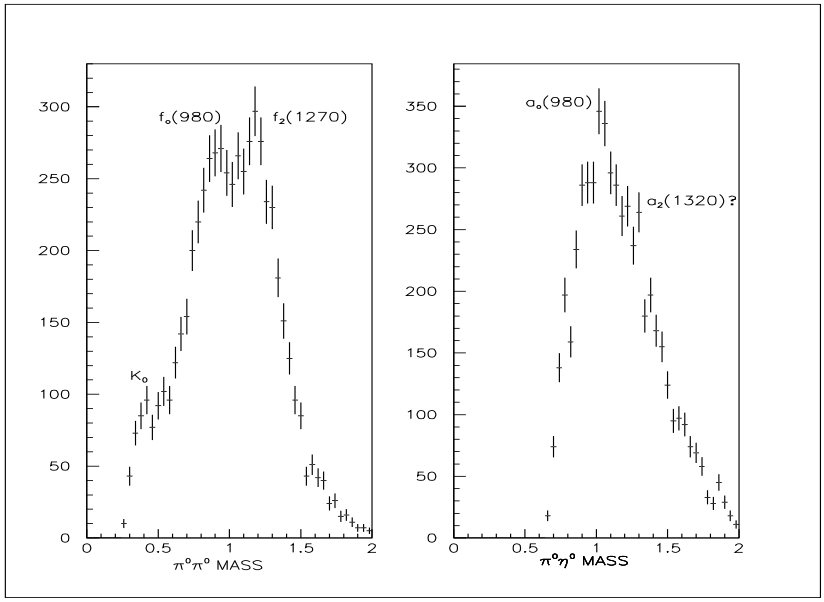

Figure 25: $\pi^0\pi^0$ and $\pi^0\eta$ invariant masses for events with only four photons in the final state. Known resonances that are possible to observe are indicated.

axis along the direction opposite to the deuteron momentum vector. This is shown schematically on the right panel in Fig. 26. The angle θ_H shown is measured in the rest frame of the K^+K^- system. The angle ϕ_H is the azimuthal angle of the hadrons relative to the γd reaction plane.

The angular distribution of the K^+K^- pair for the cosine of the helicity angle θ_H is shown in Fig. 27 for ϕ production (top) and non-resonant K^+K^- production (middle and bottom). Two different regions of the photon energy are shown (left and right), which are further subdivided into different regions of the momentum transfer t (see inset at the top). The four plots for the ϕ show the same angular distribution, and follow the curve predicted for s-channel helicity conservation. The shape of the curve, which goes like $\frac{3}{4}(1-\cos^2\theta)$, can be explained in terms of the angular momentum of the K^+K^- pair [63]. In general, the non-resonant K^+K^- angular distributions appear to follow the helicity conservation curves better for higher photon energies and for smaller $|t|$. This suggests that s-channel helicity conservation is not limited to resonance regions in forward-angle production of two spin-zero mesons, especially at higher photon energies. The azimuthal angular distributions, in the same layout as above, are shown in Fig. 28. Here, helicity conservation predicts that the distributions should be flat, as shown by the horizontal lines. Again, we see good agreement between the data and the lines at higher photon energy and small $|t|$. However, this evidence is less compelling, since there are other reasons that the azimuthal angular

distributions could be uniform. Nonetheless, if there would be serious deviation from the flat prediction, then this would indicate that s-channel helicity conservation is not dominant.

If helicity conservation holds for the non-resonant background in the proposed measurement, then this would constrain the number of PWA terms (in Eq. 7, the summation collapses and only $L = 1$ survives, see Eq. 9) that would be necessary to describe the data [10]. The data shown above are in the region $0.35 < |t| < 0.8$ GeV^2 and the proposed measurements will be at even smaller $|t|$ (see Eq. 8), below about 0.35 GeV^2. In addition, the beam energy will be at 6 GeV, providing higher virtual photon energies. If we can extrapolate from the trend of the dK^+K^- final state above, then both smaller $|t|$ and higher E_γ point in the direction of dominance of s-channel helicity conservation and hence a simpler PWA formalism.

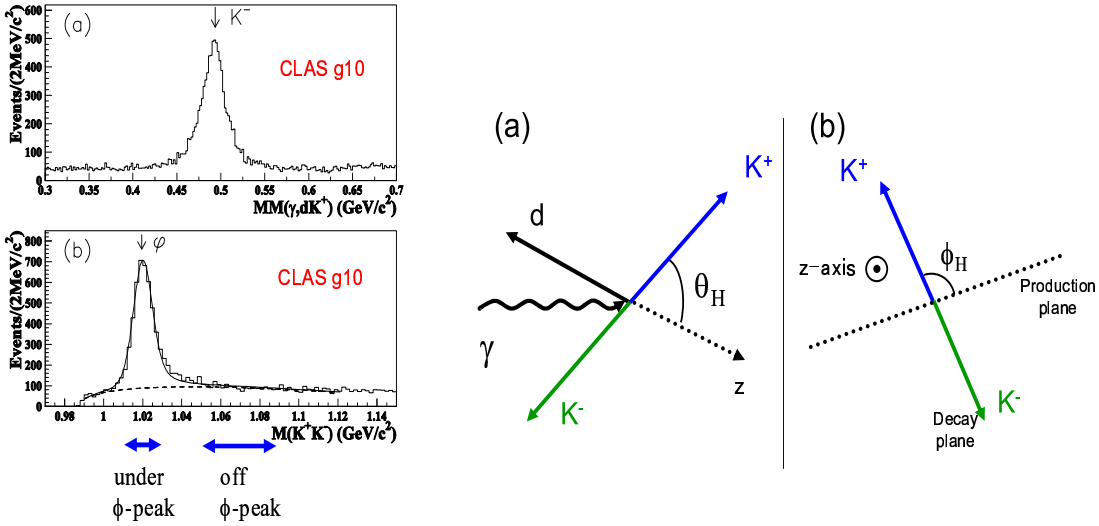

Figure 26: On the left: (a) Missing mass distribution of the reaction $\gamma d \to dK^+X$. (b) Invariant mass distribution for the K^+K^- pair after the selection of the missing K^-. The solid curve is a fit to the data. The dashed curve shows the contribution from the background. On the right: Definition of decay angles for the reaction $\gamma d \to dK^+K^-$.

8.3.2 $\pi^+\pi^-\pi^0$ final state

The main motivation for this study is to see if the difference in the three-π invariant mass distributions ($M(\pi^+\pi^-\pi^0)$) on hydrogen and on deuterium will hint at the suppression of s-channel resonance production on deuterium. The reactions $\gamma d \to \pi^+\pi^-\pi^0 d$ and $\gamma p \to \pi^+\pi^-\pi^0 p$ were studied using g10 data. Final state particles π^+, π^-, deuteron, and proton were detected in CLAS. In both reactions the π^0 kinematics

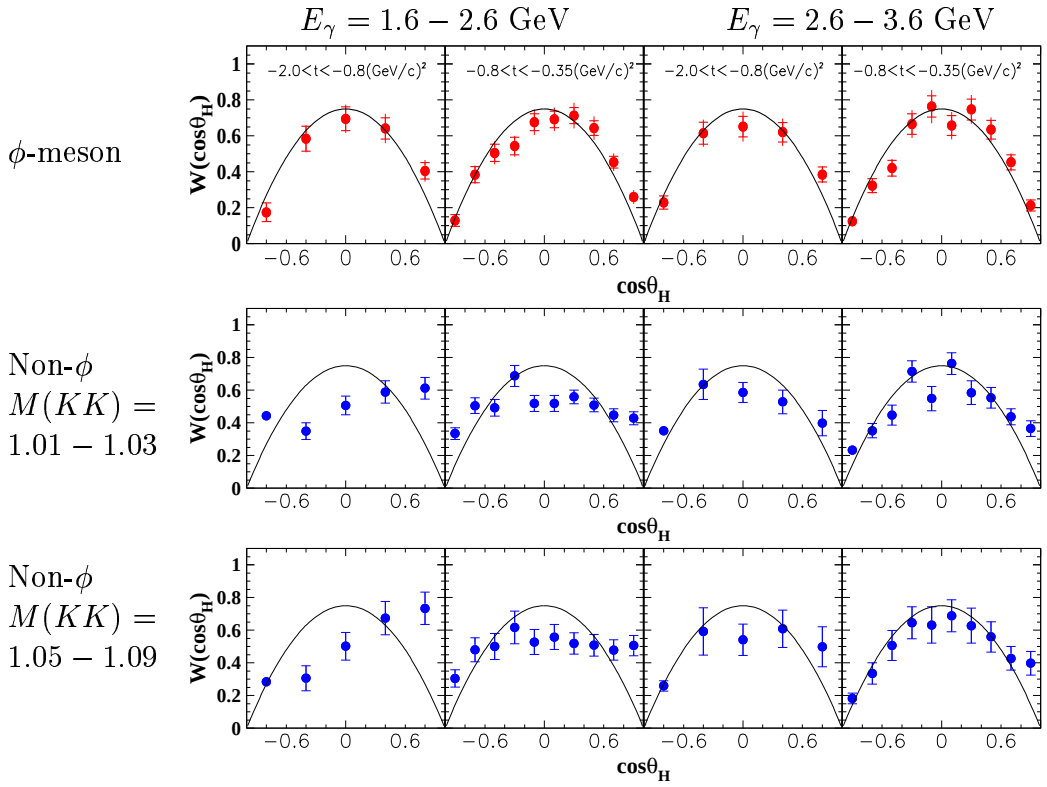

Figure 27: $\cos\Theta_H$ distributions for two energy bins and for different t-ranges.

were deduced from missing momentum analysis. Only half of the g10 data were analyzed.

In Fig. 29 $M(\pi^+\pi^-\pi^0)$ distributions for deuterium (left) and hydrogen (right) are shown. The low mass regions in both distributions are similar: the ω meson is cleanly seen, the shoulder around 1.05 GeV corresponds to $\phi \to \pi^+\pi^-\pi^0$. At higher invariant masses, $M(\pi^+\pi^-\pi^0) > 1.1$ GeV, there are interesting differences. While the distribution on the proton is smooth and structureless, following the phase space, the distribution on the deuteron shows a clear peak of the $a_2(1320)$ meson at $M(\pi^+\pi^-\pi^0) \sim 1.32$ GeV. Also structure at > 1400 MeV is visible, that can correspond to $\omega(1420)$. To fully understand the underlying structure in the $M(\pi^+\pi^-\pi^0)$ distribution in the reaction $\gamma d \to \pi^+\pi^-\pi^0 d$, analysis of angular distributions of decay mesons is necessary. Nevertheless, one way to interpret the lack of structures in the distribution on hydrogen is a large contribution of processes with nucleon resonance production, $\gamma p \to \pi N^\star(\Delta^\star)$, that make the three-$\pi$ mass distribution structureless.

One should note that the presented data are at much higher t-values than the expected data in the proposed measurement. In the coherent production at high t, rescattering processes play a significant role and so does the intermediate resonance production. In the proposed experiment, suppression of the s-channel contributions will be much improved.

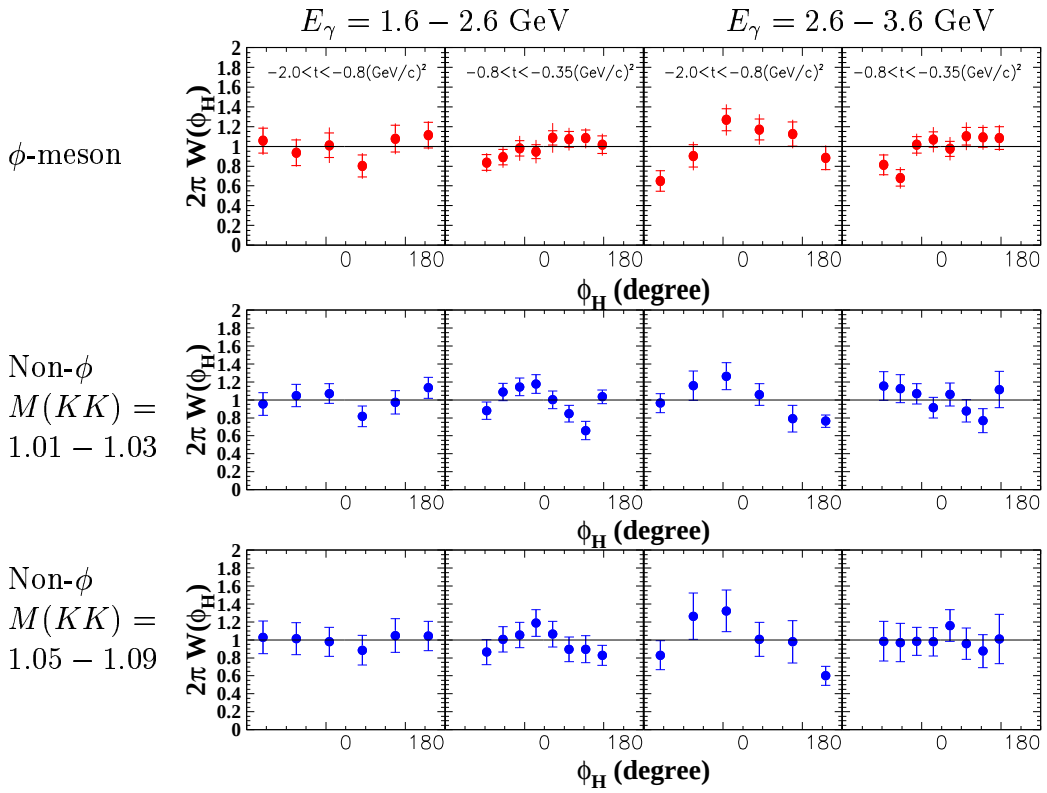

Figure 28: ϕ_H distributions for two energy bins and for different t-ranges.

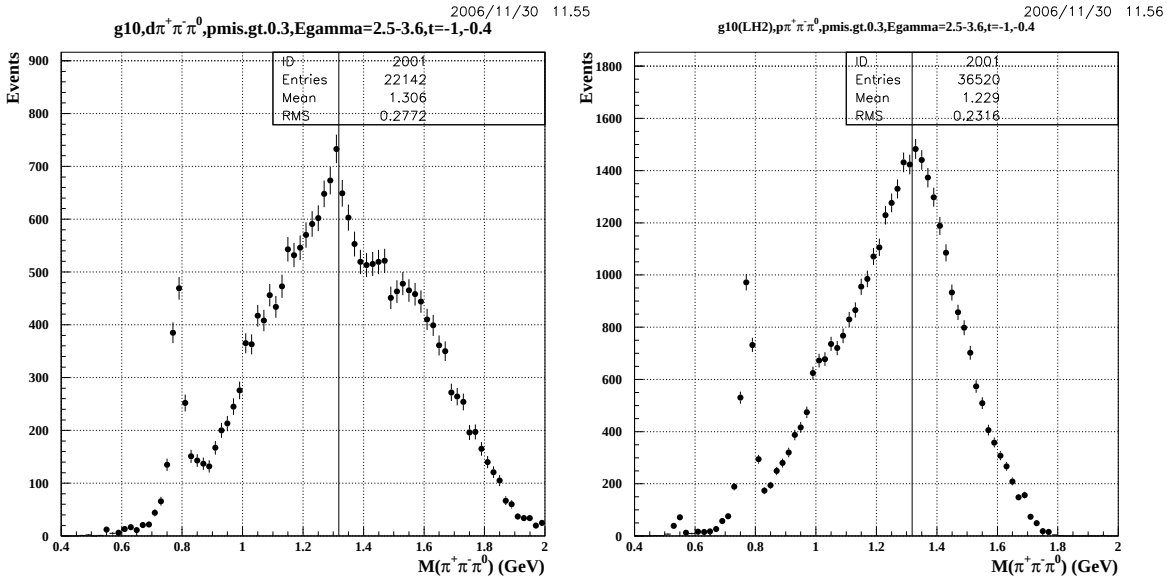

Figure 29: Invariant mass distributions of three pions in the reactions $\gamma d \to \pi^+\pi^-\pi^0 d$ (left) and $\gamma p \to \pi^+\pi^-\pi^0 p$ (right).

9 Expected Event Rate and Beam Time Request

Production rates for a_2^0 and π_1 are estimated assuming a 6 GeV electron beam and a luminosity of 3×10^{33} cm^{-2}sec^{-1}. The photoproduction cross sections presented in Section 5 are used.

9.1 Cross section for quasi-real photoproduction on ^4He

In the kinematics of this experiment ($Q^2 \to 0$) $\sigma_L \to 0$, and the cross section can be approximated as:

$$\frac{d\sigma_{eN\to eM^0N}}{dQ^2dWdt} \simeq \Gamma_W \cdot \frac{d\sigma_{\gamma N\to M^0N}}{dt}. \tag{32}$$

Here Γ_W is the flux of virtual photons and is defined as:

$$\Gamma_W = \frac{\alpha}{4\pi} \cdot \frac{W^2 - m^2}{m^2 k^{0\,2}} \cdot \frac{W}{Q^2} \cdot \frac{1}{1-\epsilon}\ . \tag{33}$$

In the equations above, ϵ is the virtual photon polarization and is given by:

$$\epsilon = \left(1 + 2\frac{Q^2 + q^{0\,2}}{4k^0k'^0 - Q^2}\right)^{-1}\ . \tag{34}$$

The other kinematical variables are: electron transferred momentum squared $Q^2 = -q^{\mu 2}$ where $q^\mu = (k^\mu - k'^\mu)$ is the four-momentum of the virtual photon, and $k^\mu(k'^\mu)$ is the four-momentum of the incoming (outgoing) electron. In Eq.(32) t is the transferred momentum squared to the target, and the total CM energy $W^2 = m^2 + 2mq^0 - Q^2$, where m is the nucleon mass.

Most of the photon flux will be generated by electrons scattered at the typical bremsstrahlung angle $\theta_e = m_e/E$ (m_e is the electron mass). Therefore, for rate calculations, we integrated Γ_W for the Q^2 range $< 10^{-4}$ (GeV/c)^2 ($\theta_e < 0.1^o$). This integrated value, as a function of photon energy is shown in Fig. 30, left panel. The relation in Eq.(32) then can be written as:

$$\frac{d\sigma_{eN\to eM^0N}}{dWdt} \simeq \Gamma \cdot \frac{d\sigma_{\gamma N\to M^0N}}{dt}. \tag{35}$$

Production on nuclei is usually used to enhance the statistics, since in that case the resulting scattering amplitude is the sum of amplitudes for scattering from individual nucleons. In the proposed experiment the gain in the production rate (cross section) compared to the scattering off a single nucleon will be a factor of 16 (assuming that production on the proton and on the neutron are equal). However, the requirement of having a ^{4}He nucleus intact will add an extra form-factor, $F_{He}(t)$ [65], in the

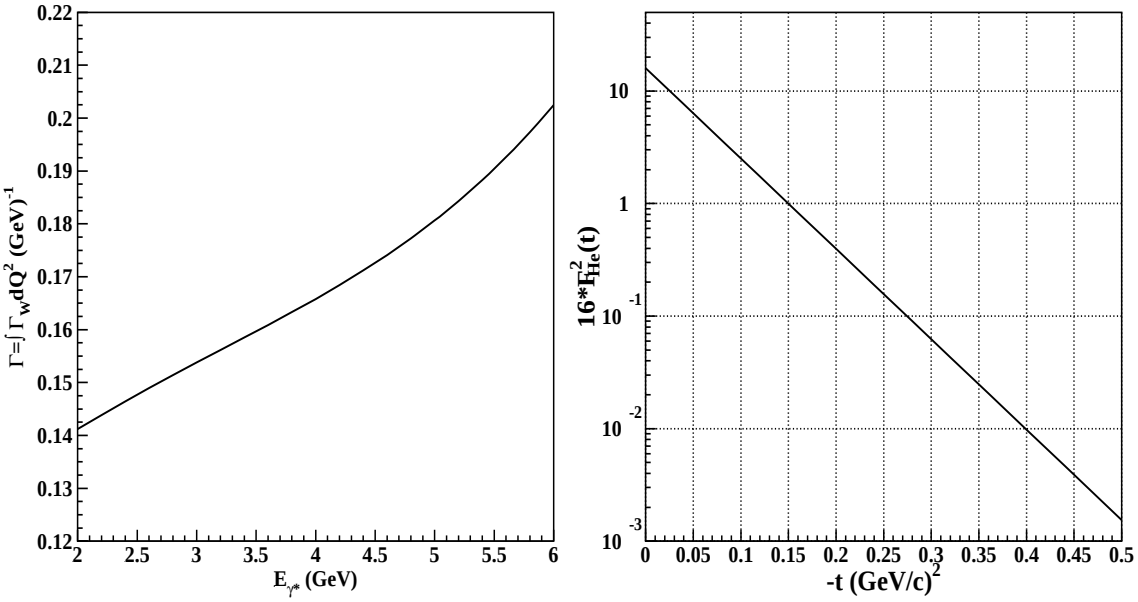

Figure 30: On the left the dependence of the integral of Γ_W over the Q^2 range $< 10^{-4}$ (GeV/c)^2 on E_γ. On the right - the factor $(A \cdot F_A(t))^2$ for ^{4}He as a function of transferred momentum squared t. The minimum momentum transferred is defined by the minimum momentum of α-particles in the RTPC and is about $|t| = 0.1$ (GeV/c)^2.

production amplitude. The cross section in Eq.(35) for the scattering on ^{4}He can be expressed as:

$$\frac{d\sigma_{eHe\to eM^0He}}{dW\,dt} \;=\; \Gamma \cdot \frac{d\sigma_{\gamma N\to M^0 N}}{dt} \cdot (4F_{He}(t))^2. \tag{36}$$

On the right panel of Fig. 30 the factor $(A \cdot F_A(t))^2$ for ^{4}He is shown as a function of the transferred momentum squared. Estimated cross sections for coherent production of $a_2^0(1320)$, $\pi_1(1400)$, and $\pi_1(1600)$ on ^{4}He (see Eq. 36) are shown in Fig. 31. The solid line corresponds to $a_2^0(1320)$ production at $< E_\gamma >= 4.3$ GeV, the dashed line corresponds to $\pi_1(1400)$ production at the same energy, and the dashed-dotted line corresponds to $\pi_1(1600)$ production at $< E_\gamma >= 5$ GeV. The values of average beam energy in each case were derived from simulations (see Section 9.2).

The minimum achievable momentum transferred is defined by the minimum momentum of α-particles in the RTPC and is about $|t| = 0.1$ (GeV/c)^2. In the event rate estimate the cross sections were integrated above that value.

9.2 Acceptances

The detector efficiency was simulated using the GEANT-3 [64] model of the CLAS detector (GSIM) and the GEANT-4 model of the BoNuS RTPC. In the event reconstruction stage, the RTPC response to α-particles from GEANT-4 simulations was

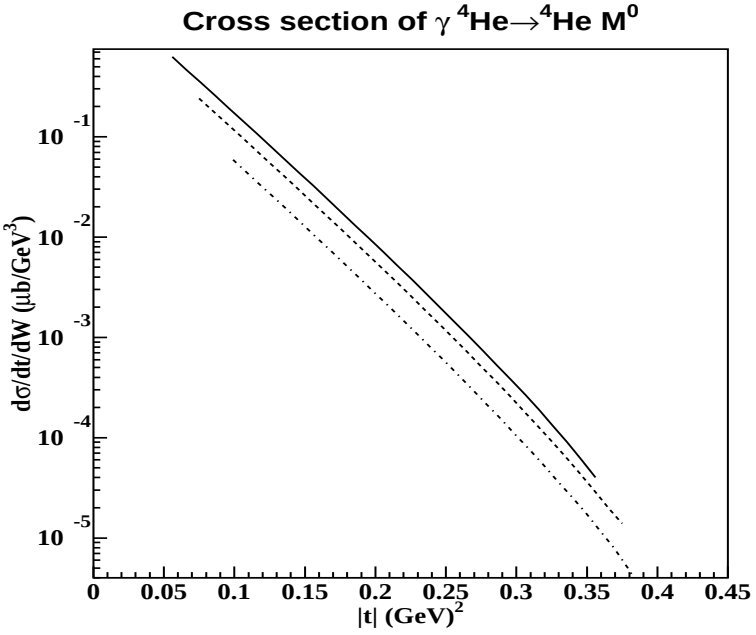

Figure 31: Cross sections for coherent production of $a_2^0(1320)$, $\pi_1(1400)$, and $\pi_1(1600)$ on ^{4}He. The solid line corresponds to $a_2^0(1320)$ production at $< E_\gamma >= 4.3$ GeV, the dashed line corresponds to $\pi_1(1400)$ production at the same energy, and the dashed-dotted line corresponds to $\pi_1(1600)$ production at $< E_\gamma >= 5$ GeV. The values of average beam energy in each case were derived from simulations. Cross sections were calculated using the value of the coupling constant $g_{\omega pp} = 14$.

parametrized and used. Events were generated using the phase space event generator FSGEN [66], with built-in t-dependence for the t-channel meson production. All decays were handled by JETSET [64], linked to FSGEN.

In Fig. 32 reconstruction of $\pi^0\eta$ final states in the reaction $\gamma^\star\ ^4He \rightarrow^4 He\ \pi^0\eta$ is shown. On the top graph the distribution of two photon invariant masses for all combinations of photon pairs in the four photon events is shown. In the reconstruction of photons both calorimeters, IC and EC, are involved. For the final event sample it was required to have at least one of the photons in the EC (a requirement for the trigger). Corresponding peaks for π^0 and η are cleanly separated.

On the bottom graph of Fig. 32 the efficiency of detection of α-particles in the RTPC and π^0s and ηs in CLAS is presented as a function of the $(\pi^0\eta)$ invariant mass. The average acceptance around $a_2^0(1320)$ and $\pi_1(1400)$ masses is about 6%.

Results of simulations of the reaction $\gamma^\star\ ^4He \rightarrow^4 He\ \pi^0\eta'$ are shown in Fig. 33, for the $\eta' \rightarrow \rho^0\gamma$ decay mode, and in Fig. 34 for $\eta' \rightarrow \pi^+\pi^-\eta$. Again, on the upper graphs

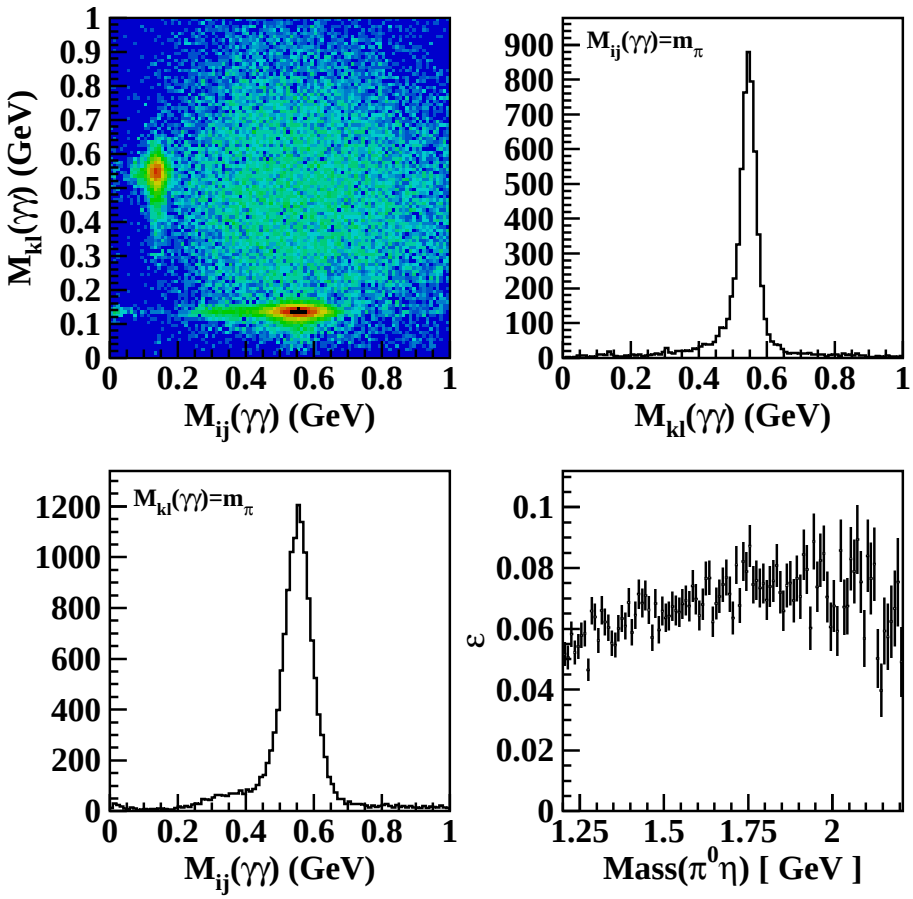

Figure 32: Reaction $\gamma^\star\ ^4He \rightarrow^4 He\ \pi^0\eta$, four photons were detected in CLAS and the α-particle was detected in the RTPC. Top left: the invariant mass of two photons (ij) vs. the invariant mass of the other two (kl), top right and bottom left are the projections, after a cut to select π^0s in one of pair. All combinations of two photons are shown. Bottom right graph - detection efficiency as a function of $M(\pi^0\eta)$.

of both figures, reconstruction of the final state particles is shown. On the lower graphs, the efficiencies of detection as a function of M$(\pi^0\eta')$ are presented. Detection efficiencies are 0.7% and 0.3% for the decay modes $\eta' \rightarrow \rho^0\gamma$ and $\eta' \rightarrow \pi^+\pi^-\eta$, respectively.

The angular distributions of reconstructed π^0s in the Gottfried-Jackson frame for the reactions $\gamma^\star\ ^4He \rightarrow^4 He\ \pi^0\eta$, the top panel, and $\gamma^\star\ ^4He \rightarrow^4 He\ \pi^0\eta'$, the bottom panel, are shown in Fig. 35. There are no acceptance holes in ϕ_{GJ} for either reaction. For the $\pi^0\eta$ final state, the effect of the torus coils is seen at the level of 20%. This is when both photons from π^0 decay were detected in the CLAS forward calorimeter. For the case of the $\pi^0\eta'$ final state, the distributions are smoother.

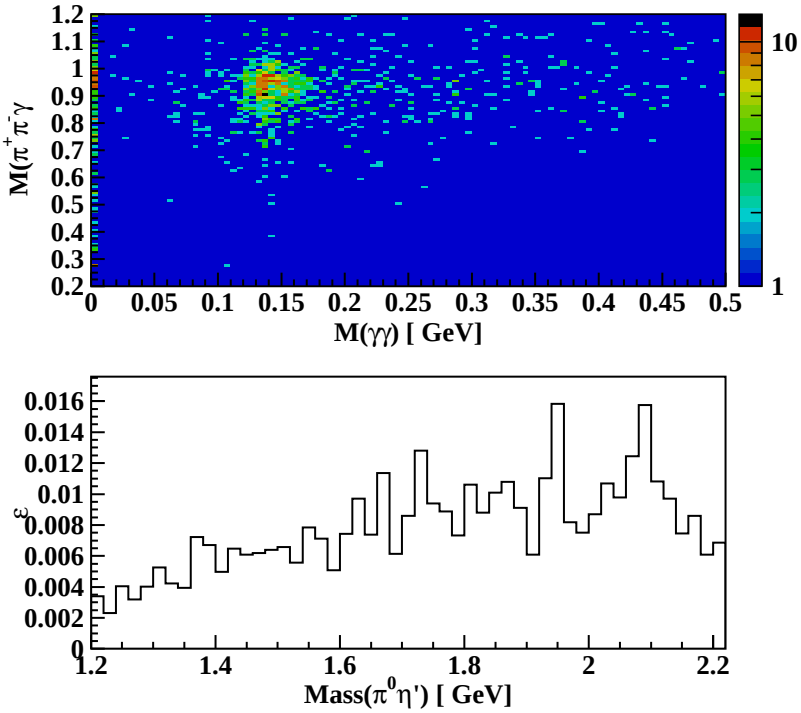

Figure 33: Reaction $\gamma^{\star}\ ^4He \rightarrow ^4\ He\ \pi^0\eta'$, $\eta' \rightarrow \rho^0\gamma$. Three photons, π^+, and π^- were detected in CLAS and the α-particle was detected in the RTPC. The upper graph shows reconstruction of η' and π^0. The bottom graph shows the efficiency of the detection vs. M($\pi^0\eta'$).

9.3 Event rate

The cross sections presented in Fig. 31 were used to calculate production rates for $a_2^0(1320)$, $\pi_1(1400)$, and $\pi_1(1600)$. These cross sections were calculated using $g_{\omega pp} = 14$ from [44]. If the value of $g_{\omega pp} = 21$ from Ref. [49] is used, then the cross sections will be a factor of 2 higher. In order to estimate the expected rate for π_1^0 production in the $\pi^0\eta$ and $\pi^0\eta'$ channels, it is necessary to know the branching ratios $Br(\pi_1^0 \rightarrow \pi^0\eta)$ and $Br(\pi_1^0 \rightarrow \pi^0\eta')$. Although the $\eta\pi$ width of π_1 is suppressed by symmetrization rules (see, for example, Ref. [53]) and has been estimated in different QCD approaches to be tiny, in Ref. [42] it is shown that final state interactions can produce $\Gamma(\pi_1 \rightarrow \pi\eta) = 57 \pm 14\ MeV$. Considering the measured widths of the $\pi_1(1400)$ of 380 MeV [28] and the $\pi_1(1600)$ of 185, we used a conservative values for the branching ratios: $\Gamma(\pi_1 \rightarrow \pi^0\eta) = 0.1$ and $\Gamma(\pi_1 \rightarrow \pi^0\eta') = 0.3$.

Other branching ratios used in the calculations are: $\Gamma(\pi^0 \rightarrow \gamma\gamma) = 0.99$, $\Gamma(\eta \rightarrow \gamma\gamma) = 0.4$, $\Gamma(\eta' \rightarrow \rho\gamma) = 0.3$, $\Gamma(\eta' \rightarrow \pi^+\pi^-\eta) = 0.44$, $\Gamma(\rho \rightarrow \pi^+\pi^-) = 1$.

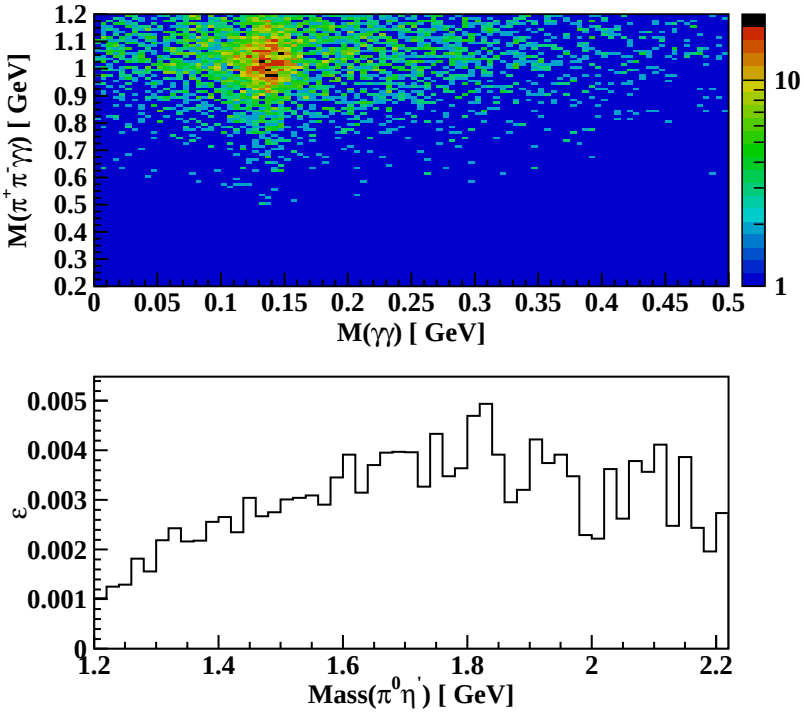

Figure 34: Reaction $\gamma^\star\ ^4He \rightarrow ^4\ He\ \pi^0\eta'$, $\eta' \rightarrow \pi^+\pi^-\eta$. Four photons ($\pi^0\eta$), π^+, and π^- were detected in CLAS and the α-particle was detected in the RTPC. The upper graph shows reconstruction of η' and π^0. The bottom graph shows the efficiency of the detection vs. M($\pi^0\eta'$).

The expected number of events was calculated as:

$$N_{a_2^0} = \Gamma \cdot \frac{d\sigma_{\gamma N \rightarrow M^0 N}}{dt} \cdot (4F_{He}(t))^2 \Delta W \cdot \Delta t \cdot L \cdot \epsilon \cdot Br_{M^0} \cdot Br_m, \tag{37}$$

where ΔW and Δt are the bin sizes for the total energy and transferred momentum squared, $L = 3 \times 10^{33}$ cm^{-2}sec^{-1} is the luminosity, and ϵ is the detection efficiency for the given final state. In Eq.(37) Br_{M^0} is the branching ratio of $a_2^0(1320)$, $\pi_1(1400)$, and $\pi_1(1600)$ to a given final state and Br_m is the combined branching ratio of the other final state meson decays.

Table 1 summarizes values of ΔW, Δt, and ϵ for different particles and different decay modes. Expected event statistics for 45 days of running at luminosity of $L = 3{\times}10^{33}$ cm^{-2}sec^{-1} for various reactions are shown in Table 2. We expect to reconstruct more than 50000 $a_2^0 \rightarrow \pi^0\eta$ decays, about 36000 $\pi_1(1400) \rightarrow \pi^0\eta$ decays, and about 15500 decays of $\pi_1(1600) \rightarrow \pi^0\eta$. We will collect more than 5000 $\pi_1(1600)$ in the $\pi^0\eta'$ mode. These expectations are based on the cross sections calculated with $g_{\omega pp} = 14$. For the more optimistic estimate, $g_{\omega pp} = 21$, statistics will be higher by a factor of 2 (see Table 2).

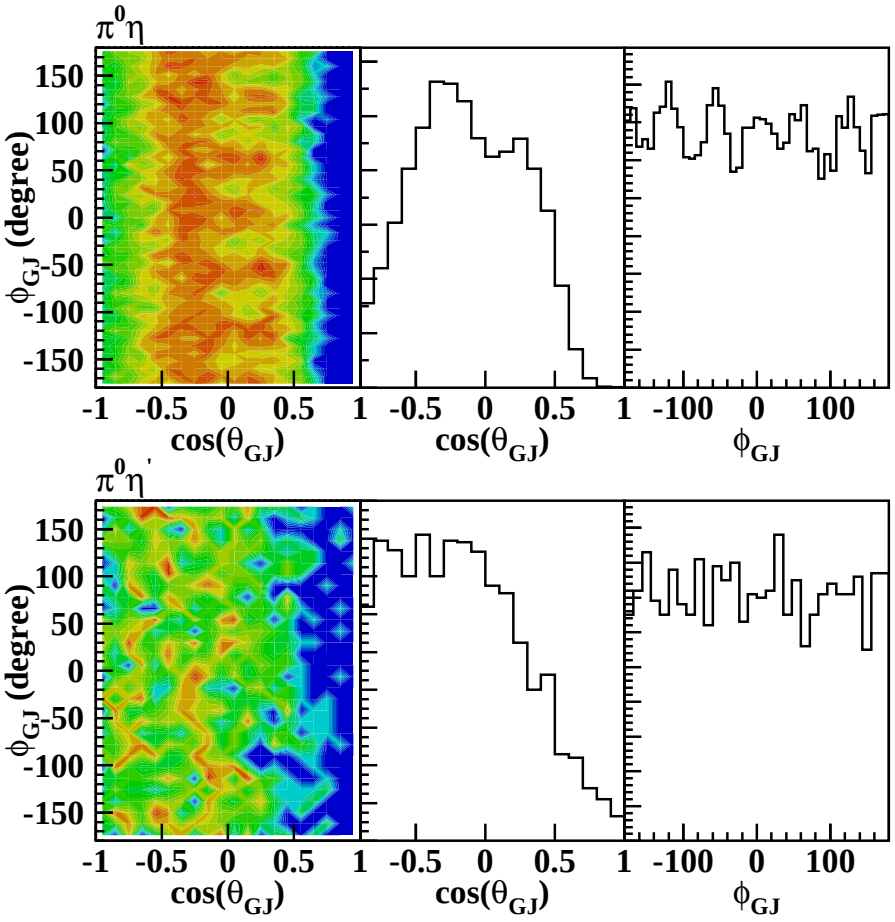

Figure 35: Angular distributions of the π^0 in the GJ frame for the reactions $\gamma^\star\ ^4He \rightarrow ^4He\ \pi^0\eta$ (top panel) and $\gamma^\star\ ^4He \rightarrow ^4He\ \pi^0\eta'$ (bottom panel).

Meson, M^0	ΔW (GeV)	Δt (GeV/c)^2	ϵ
$a_2^0(1320) \rightarrow \pi^0\eta$	0.25	0.15	0.06
$\pi_1^0(1400) \rightarrow \pi^0\eta$	0.25	0.15	0.06
$\pi_1^0(1600) \rightarrow \pi^0\eta$	0.2	0.1	0.07
$\pi_1^0(1600) \rightarrow \pi^0\eta'(\rho\gamma)$	0.2	0.07	0.007
$\pi_1^0(1600) \rightarrow \pi^0\eta'(\pi^+\pi^-\eta)$	0.2	0.07	0.003

Table 1: Bin sizes (ΔW and Δt) and the detection efficiencies (ϵ) for the $a_2^0(1320)$, $\pi_1(1400)$, and $\pi_1(1600)$ in different decay modes.

Meson, M^0	$M^0 \to \pi^0\eta$	$M^0 \to \pi^0\eta'$
$a_2^0(1320)$	53000 [106000]	-
$\pi_1^0(1400)$	36000 [72000]	-
$\pi_1^0(1600)$	15500 [31000]	3600 [7200] ($\eta' \to \rho^0\gamma$) 1500 [3000] ($\eta' \to \pi^+\pi^-\eta$) 5100 [10200] (total)

Table 2: Expected statistics during 45 days of running for coherent production of $a_2^0(1320)$, $\pi_1(1400)$, and $\pi_1(1600)$ in the reaction $\gamma^\star\ {}^4He \to\ {}^4HeM^0$ with a 6 GeV beam and a luminosity of $L = 3{\times}10^{33}$ cm^{-2}sec^{-1}. In the square brackets are estimates when $g_{\omega pp} = 21$ was used.

10 Summary

QCD based models allow the existence of hybrids, hadrons with an explicit gluonic degree of freedom. Hybrid mesons can have exotic J^{PC} or J^{PG} quantum numbers, different from those of a $q\overline{q}$ pair. Mesons with exotic quantum numbers offer a unique signature for hybrids.

This experiment will search for a $J^{PC} = 1^{-+}$, $J^{PG} = 1^{--}$ exotic signal in the coherent electroproduction off ^{4}He using the Hall B CLAS detector. The mass range of $\pi^0\eta$ and $\pi^0\eta'$ up to $\approx$ 2 GeV will be explored. The $J^{PC} = 1^{-+}$ exotic will be unambiguously reconstructed through the analysis of the decay angular distributions of the final state mesons. The zero spin and isospin of the target will dramatically simplify the Partial Wave Analysis. There will be no background from s-channel nucleon resonances.

In 45 days of running with a 20 cm long, 7 atm ^4He gas target with a 6 GeV electron beam at 130 nA current, we will collect 53000 $a_2^0 \to \pi^0\eta$ events, about 36000 events from an exotic $J^{PC} = 1^{-+}$ state, $\pi_1(1400)$, decaying to $\pi^0\eta$. The $\pi_1(1600)$ will be reconstructed in two decay modes: $\pi^0\eta$ and $\pi^0\eta'$, and we expect statistics in these decay modes to be 15500 and 5100, respectively.

Let us note, that although the main focus of the proposed measurements are the reactions presented in Eq.(1) and Eq.(2), due to the open acceptance of CLAS many other final states will be recorded in parallel. For the reasons stated above, the coherent production on ^{4}He will put constraints on the production mechanism of different final states and will simplify the PWA analysis. This will allow us to extend the studies of exotic states to other decay modes, see e.g. Section 13.

11 Appendix I: BoNuS RTPC readout

The Radial Time Projection Chamber built for the BoNuS experiment consists of two half-cylinder TPC's, each featuring 1,600 readout pads on the outermost shell (readout plane), for a total of 3,200 pads. Groups of 16 pads are traced to a common connector on the readout plane, which supports a circuit board with 16 individual pre-amplifier channels with a gain of about -1. The amplified signals are sent over a five meter long flatband cable to 128-channel receiver cards in a pseudo-VME format. The receiver cards feature 8×16 channels of impedance-matched receiver channels, which feed the signals into the piggyback mounted Front End Cards (FEC's). These readout cards are the standard readout for the ALICE TPC and were bought from CERN. The 8×16 channels of pre-amplification and shaping (PASA) and eight custom ALTRO chips, each provide 16 channels of pedestal subtraction, baseline corrections, 10-bit digitization, and up to eight buffers organized in a ring structure. The receiver cards also supply the power to the amplifier/inverter cards and to the FEC. A group of 13 FEC/receiver cards is needed to read out one half-cylinder of the RTPC. The 13 cards are controlled via a data bus and a control bus by a readout controller, U2F. The U2F transmits the data via USB2.0 to a PC or VME crate controller and also provides the software download and features user-programmable output ports, like a busy feedback. At the present time, the firmware of the U2F controller does not support the eight buffer pipeline and, hence, can only be used in an event-by-event readout scheme (ROC-lock mode) when used in conjunction with the CLAS detector. This limits the DAQ rate to presently about 500 Hz.

The U2F controller is not the standard readout controller of the ALICE TPC FEC's. It is used for a limited number of FEC's in a practical and small package, easily connected to a laptop USB2.0 port. The standard Readout Control Unit (RCU) is using the buffer feature of the FEC's. It is possible to upgrade the existing U2F firmware to add this feature. This upgraded firmware has to be developed and tested at CERN. It is presently scheduled for December 2006 release, given that there are no further setbacks of the installation of the ALICE TPC. The improved rate is expected to be at least 1 kHz. No purchases are necessary.

12 Appendix II: Neutral trigger rate estimate

The trigger rate estimate was done using the DVCS inner calorimeter (IC) [60] calibration and production runs from the e1-DVCS experiment. The IC calibration data were acquired using a setup that was triggered by a high energy deposition in the IC. The original electronic logic of the IC was not designed to have an accurate trigger. Signals from all 424 IC channels were split with a ratio of 1:2 and the largest portion of the signal was sent to discriminators. Two outputs of the discriminators were used for scalers and for TDCs. The 16 channel Lecroy discriminators had one threshold for all inputs. The discriminator generated an additional signal on the back

panel, that was proportional to the number of channels that had input signals above the threshold. These signals from all boards were used to generate the trigger signal from the IC.

Of course due to the gain variations in the individual crystal counters and a single threshold for 16 channels, this system did not generate a sharply defined trigger threshold. But, it was good enough to trigger on high energy deposition in the IC (> 3 GeV) for the detector calibration. In the top graph of Fig. 36 the distribution of events as a function of the total energy in the IC for a calibration run at 20 nA is shown. The 20 nA beam current corresponds to $\sim 1.5 \times 10^{34} cm^{-2} sec^{-1}$ luminosity. The trigger rate during this run was ~ 8.5 kHz. In the lower graph of Fig. 36, the IC energy distribution is shown, when in addition to the energy detected in the IC an energy > 0.07 GeV (equivalent to the ~ 0.2 GeV photon) was detected in one of the CLAS forward electromagnetic calorimeters. This coincidence reduces the number of events, and hence the event rate, by a factor of 20. However during these runs, only 3 sectors of the EC were read out, so the real rate for $IC \times EC$ coincidences will be ~ 0.85 kHz at $L_C = 1.5 \times 10^{34} cm^{-2} sec^{-1}$.

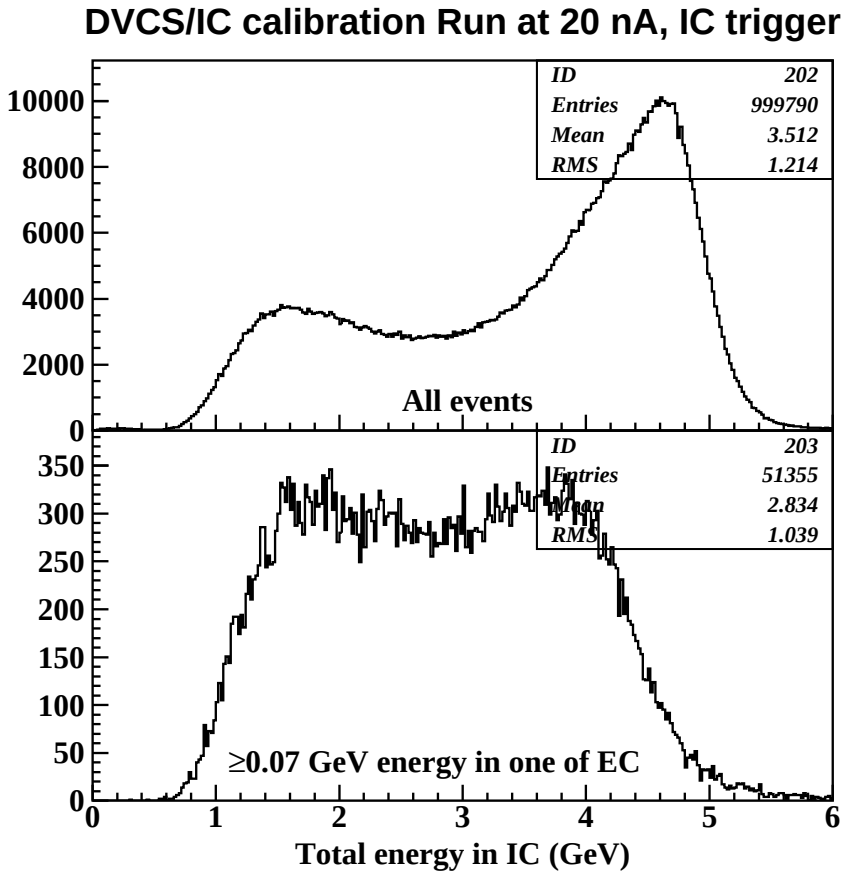

Figure 36: Energy distribution in the IC from e1-DVCS calibration data.

For the proposed experiment a better trigger system for the IC is required. Two

trigger settings were studied for the experiment: (1) $E_{IC} > 0.5$ GeV energy in the IC in coincidence with $E_{EC} > 0.07$ GeV energy in one of the forward EC $[IC(> 0.5 \times EC_i(> 0.07), i = 1, 6]$; (2) > 0.07 GeV energy in any two forward EC modules $[EC_i(> 0.07) \times EC_j(> 0.07), i \neq j]$. The rates of such trigger setups were studied using the DVCS production and IC calibration runs. Events with multiple photons and a positive track, but no electron detected in CLAS, were used from the production run. It was found that the number of events with setting (1) was an order of magnitude higher than the number of events in setting (2). To estimate the trigger rate with setting (1), the IC energy distributions from production and calibration runs were compared. It was assumed that the trigger in the IC calibration runs did not affect the energy spectrum in the IC in the high energy range, $E_{IC} > 3$ GeV. So the normalization of event rate was done by comparing energy spectra at > 4 GeV.

In Fig. 37, the energy distribution in the IC is shown for events from a production run selected with a positive track and multiple photons ($n_\gamma > 3$). It was required to have > 0.07 GeV energy in one of the EC modules. No negative track was reconstructed in these events. The normalized distribution for the IC calibration run (distribution in the lower panel of Fig. 36) is shown with the dashed histogram. In the energy range above 1 GeV, where most of the events in the calibration run are, the number of events in the production run (not effected by the IC trigger) is about 6 times higher than the number events in the dashed histogram. Therefore, it is expected to have 6 times higher trigger rate for a proper trigger configuration with trigger energy > 1 GeV. Consequently, for the proposed trigger threshold, > 0.5 GeV, the rate is expected to be 13 times higher than for the calibration trigger with an extra energy deposition of > 0.07 GeV in one of the forward EC modules. This means that for the luminosity of $L = 1.5 \times 10^{34} cm^{-2} sec^{-1}$, with the proper trigger setting, with IC energy > 0.5 GeV, the expected trigger rate will be $13 \times 0.85 kHz \sim 11 kHz$.

A new trigger setup for the IC will have more flexibility to select modules and to set the thresholds in the trigger logic. Since the inner most crystals will be mostly hampered by an electromagnetic background (e.g. Moller electrons), we plan to leave out these modules from the trigger setup. In this case the normalized number of events in the energy range > 0.5 GeV will be only 333 K, see Fig. 38. This corresponds to an event rate of ~ 5.5 kHz at luminosity of $L_C = 1.5 \times 10^{34} cm^{-2} sec^{-1}$.

Minimal improvements to the BoNuS RTPC electronics will allow us to run at readout rate of about 1 kHz. This will set the limit to the acceptable luminosity for the experiment at $L = L_C/5.5 \simeq 2.7 \times 10^{33} cm^{-2} sec^{-1}$.

13 Appendix III: Search for exotic mesons in the $\phi\pi$ final state

One very attractive method to identify exotic mesons is through the $\phi\pi$ decay mode. Any $s\bar{s}$-meson decay to $\phi\pi$ is forbidden due to the conservation of isotopic

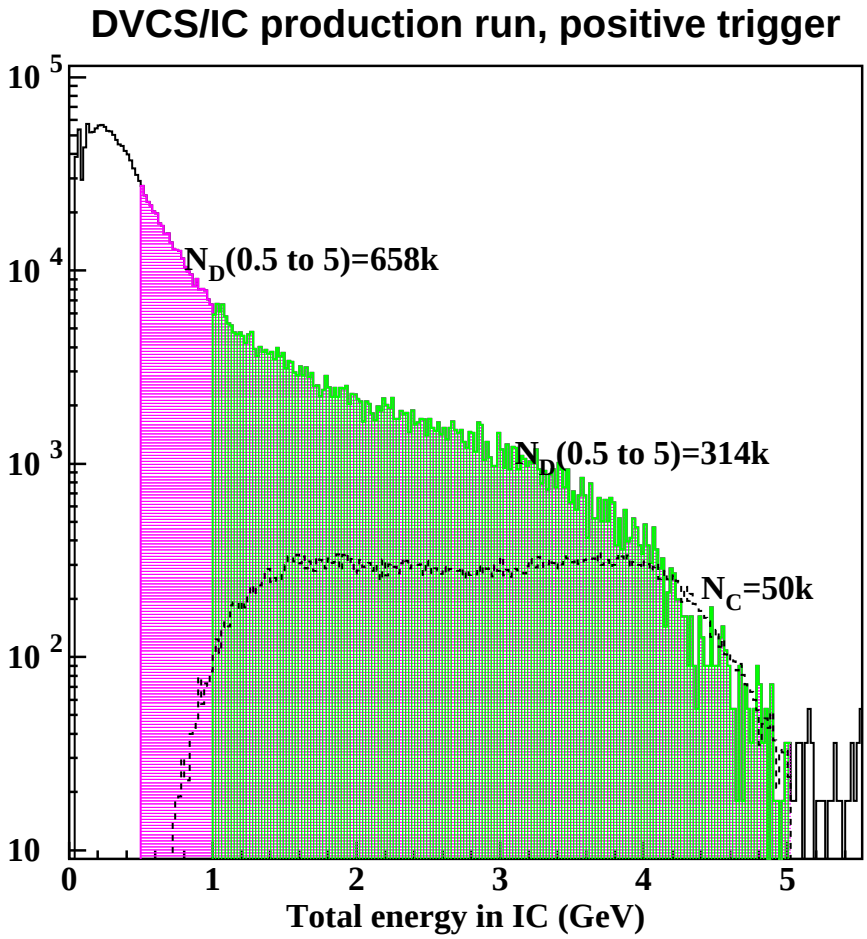

Figure 37: Rate distribution as function of total energy in IC for events without electron (positive trigger). N_D is the number of events in the production run, N_C is the number of events in the calibration run with IC trigger.

spin. This decay mode is forbidden by the Okubo-Zweig-Iizuka (OZI) rule for any $n\bar{n}$-meson (where n is a u or d quark) as well. On the other hand, multi-quark or hybrid mesons may have a strong coupling to the $\phi\pi$ system. The discovery of a $\phi\pi$ resonance would indicate a new kind of hadron and suggest a $q\bar{q}g$ or $q\bar{q}q\bar{q}$ state. This is true for $f'\pi$ and $\psi\pi$ decay modes as well [67].

There is some experimental evidence for the existence of a resonance with strong $\phi\pi$ coupling. In experiments at the LEPTON-F spectrometer [68, 69] the charge exchange reaction

$$\pi^- p \to (\phi\pi^0)n, \tag{38}$$

has been studied at a π^-–momentum of 32 GeV/c. In the mass spectrum of the $\phi\pi^0$ system a new meson, C(1480), with mass 1480 ± 40 MeV and width 130 ± 60 MeV, was observed. The angular distributions of the sequential decay $C(1480) \to \phi\pi^0, \phi \to K^+K^-$ have been studied, and the quantum numbers for the C(1480) meson have been determined: $I^G = 1^+, J^{PC} = 1^{--}$. For this meson an anomalously large value

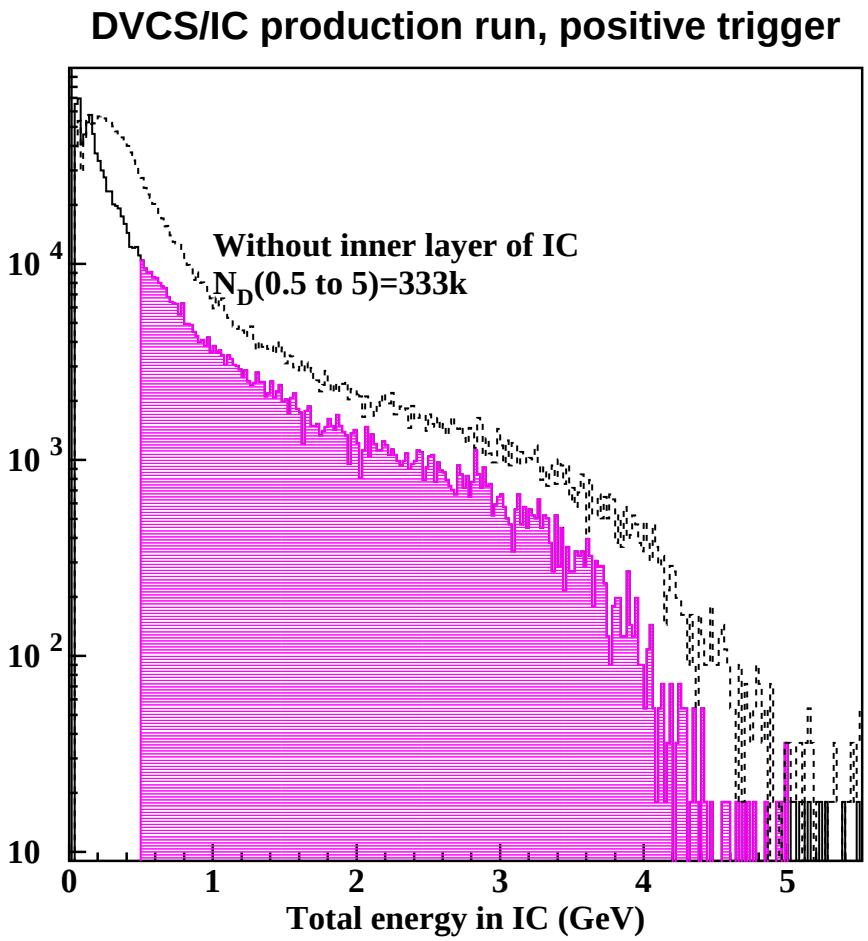

Figure 38: Rate distribution as function of total energy in IC for events without electron (positive trigger).

of the ratio

$$BR(C(1480) \to \phi\pi^0)/BR(C(1480) \to \omega\pi^0) > 0.5 \tag{39}$$

at 95% C.L. has been obtained. This value is more than two orders of magnitude higher than the expected ratio for mesons with the standard isovector quark structure. At the present time the only consistent explanation of these properties can be obtained with the assumption that the $C(1480)$ meson is a four quark or hybrid state.

At the Ω–spectrometer [70] the cross section for the reaction $\gamma p \to \phi\pi^0 p$ has been measured. Although the number of events is not large ($\sim$ 25), an excess of events in the mass spectrum of the $\phi\pi^0$ system at $\sim$1.4 GeV is observed. The $\phi\pi^0$ photoproduction cross section was estimated as

$$\sigma(\gamma p \to \phi\pi^0 p) = 6 \pm 3 \text{ nb} \tag{40}$$

(at 95% C.L.). The existence of the structure in the same mass range was confirmed with the study of inclusive $\phi\pi^+$ production with a pion beam [71].

Photoproduction (or low Q^2 electroproduction) is likely to be one of the more promising mechanisms for the production of exotic mesons with hidden strangeness due to the relatively large $s\bar{s}$ content of the photon. Photons are also expected to be efficient in the production of spin-1 hybrids.

The CLAS spectrometer has excellent momentum and angular resolution and particle identification. The first attempts to explore existing CLAS data from the runs g6a and g6b showed that the multi-particle reactions

$$\gamma p \to (\phi\pi^0)p, \quad \phi \to K^+K^-, \quad \pi^0 \to \gamma\gamma \tag{41}$$

$$\gamma p \to (\phi\pi^+)n, \quad \phi \to K^+K^- \tag{42}$$

can be investigated successfully [72]. In the production on a nucleon the main background to the mesonic states that decays to $\phi\pi$ comes from the excitation of baryon resonances, e.g.

$$\gamma^* p \to \phi\Delta, \quad \Delta \to p\pi^0. \tag{43}$$

Coherent production of $\phi\pi^0$ on ^{4}He is a powerful tool to suppress background from any isobar excitations, and a resonance produced in the reaction:

$$\gamma^* \, {}^4He \to \phi\pi^0 \, {}^4He, \quad \phi \to K^+K^-, \quad \pi^0 \to \gamma\gamma \tag{44}$$

will be an exotic state.

References

[1] F. de Viron and J. Weyers *Nucl. Phys. B185*, 391 (1981). T. Barns, F.E. Close, and F. de Viron, *Nucl. Phys. B224*, 241 (1983).

[2] M. Chanowitz and S. Sharpe, *Nucl. Phys. B222*, 211 (1983).

[3] N. Isgur and J. Paton, Phys. Rev. D **31**, 2910 (1985).

[4] I.I. Balitsky, D.I. Dyakonov and A.V. Yung, *Z Phys. C33*, 265 (1986)

[5] F. E. Close and P.R. Page, Nucl.Phys. **B443**, 223 (1995).

[6] P. R. Page, Phys.Lett. **B402**, 183 (1997).

[7] F. E. Close and J. J. Dudek, Phys.Rev. **D70**, 094015 (2004).

[8] C. Michael, hep-lat/0302001 (2003).

[9] J.N. Hedditch *et al.*, hep-lat/0510103 (2005).

[10] I.G. Aznauryan, Z.Phys. C 68, 459 (1995).

[11] C. Morningstar, nucl-th/0308026; AIP Conf. Proc. **698**, pp. 530-534 (AIP, New York, 2003).

[12] N. Mathur *et al.*, Phys. Lett. bf B 605, 137 (2005).

[13] M. Nozar, CLAS-ANALYSIS 2006-102 (2006).

[14] P. Eugenio, C. Salgado and D. Weygand, Experiment E04-005 (2005).

[15] L. G. Landsberg, Physics of Atomic Nuclei, Vol. 57, 42 (1994).

[16] T. Barnes, hep-ph/0007296.

[17] C. Amsler, N. Tornqvist, Physics Reports **389**, 117 (2004).

[18] N. Isgur, R. Kokoski and J. Paton, *Phys. Rev. Lett. 54*, 869 (1985).

[19] S.Taun *et al.*, Phys. Lett. **B213**, 537 (1988).

[20] M.Tanimoto Phys. Rev **D27**, 2648 (1983).

[21] C. W. Bernard *et al.* [MILC Collaboration], Phys. Rev. D **56**, 7039 (1997) [arXiv:hep-lat/9707008].

[22] M. S. Cook, H. R. Fiebig, Phys.Rev. **D74**, 034509 (2006).

[23] T.J. Barnes and F.E. Close, hep-ph/0604161 (2006).

[24] D. Alde *et al.*, Phys. Lett. **B205**, 397 (1988).

[25] Y.D. Prokoshkin and S.A. Sadovskii, Physics of Atomic Nuclei **58**, 606 (1995).

[26] G.M. Beladidze *et al.*, Phys. Lett. **B313**, 276 (1993).

[27] H. Aoyagi *et al.*, Phys. Lett. **B314**, 246 (1993).

[28] D.R. Thompson *et al. (E852 Collaboration)*, Phys. Rev. Lett. **79**, 1630 (1997).

[29] A. Abele *et al.*, Phys. Lett. **B423**, 175 (1998); Phys. Lett. **B446**, 349 (1998).

[30] Particle Data Group, J. Phys. **G 33**, 1 (2006).

[31] A.P. Szczepaniak *et al.*, Phys. Rev. Lett. **91**, 092002 (2003).

[32] A.R. Dzierba *et al.*, Phys. Rev. D **67**, 094015 (2003).

[33] Y. Khokhlov *et al.* (*VES Collaboration)*, Nucl. Phys. A **663**, 596 (2000).

[34] G.S. Adams *et al.*, Phys. Rev. Lett. **81**, 5760 (1998).

[35] A. P. Szczepaniak *et al.* Phys.Rev. **D69**, 051901,2004.

[36] S. U. Chung, E. Klempt, J. G. Korner, Eur.Phys.J. **A15**,539-542,2002.

[37] F. E. Close, Harry J. Lipkin, Phys.Lett. **B196**, 245,1987.

[38] E.I. Ivanov *et al. (E852 Collaboration)*, Phys. Rev. Lett. **86**, 3977 (2001).

[39] J. Kuhn *et al. (E852 Collaboration)*, Phys. Lett. B **595**, 109 (2004).

[40] M. Lu *et al.* (*E852 Collaboration)*, Phys. Rev. Lett. **94**, 032002 (2005).

[41] A. Dzierba *et al.*, Phys. Rev. D **73**, 072001 (2006).

[42] A. Donnachie and P. R. Page, Phys.Rev. **D 58**, 114012 (1998).

[43] J. Dudek and A. Szczepaniak, JLAB-THY-05-434 (2006)

[44] O.Dumbrajs *et al.*, *Nucl. Phys. B216*, 277 (1983).

[45] M. Guidal, J-M. Laget, M. Vanderhaegen, Nucl.Phys. **A627**, 645 (1997).

[46] G. Arakelyan, A. Grigoryan, N. Ivanov, Yad.Fiz. **51**, 1665 (1990).

[47] I. Aznauryan, Yad.Fiz. **60**, 666 (1997).

[48] B.J. Hartley and G.L. Kane, Nucl.Phys. **B 57**, 157 (1973).

[49] D.Drechsel, O.Hanstein, S.S.Kamalov, L.Tiator, Nucl.Phys. **A645**, 145 (1999).

[50] F. E. Close and J. J. Dudek, Phys.Rev. **D52**, 1706 (1995).

[51] F. E. Close and P. R. Page, Phys.Rev. **D52**, 1706 (1995).

[52] P. R. Page, E. S. Swanson, A.Szczepanyak, Phys.Rev. **D59**, 034016 (1999).

[53] P. R. Page, Phys.Lett. **B401**, 313 (1997).

[54] T.H Bauer, R.D. Spital, and D.R. Yennie, Reviews of Modern Physics, Vol 50, No. 2 (1978).

[55] Y. Eisenberg *et al.*, Phys. Rev. Lett. **23**, 1322 (1972).

[56] Y. Eisenberg *et al.*, Phys. Rev. D **5**, 15 (1972).

[57] S. U. Chung *et al.*, Phys.Rev. **D60**, 092001 (1999).

[58] C. Keppel, S. Kuhn, W. Melnitchouk, and H. Fenker, CLAS experiment E-03-012 (2003).

[59] V. Burkert, L. Elouadrhiri, M. Garçon, S. Stepanyan, CLAS experiment E-01-113 (2001).

[60] R. Niyazov and S. Stepanyan, CLAS-NOTE 2005-021 (2005).

[61] F.-X. Girod, CLAS-NOTE 2005-023 (2005).

[62] T. Mibe *et al.*, CLAS g10 analysis (2006)

[63] K. Schilling, P. Seyboth and G. Wolf, Nucl. Phys. B15, 397 (1970)

[64] CERN program library (2003).

[65] H.Morita and T.Suzuki, Progress of Theoretical Physics V.86 N.3, 671 (1991).

[66] S. Stepanyan, Phase space event generator (CLAS softwar library).

[67] F.E. Close and H.J. Lipkin, *Phys. Rev. Lett.* **41**, 1263 (1978).

[68] S.I. Bityukov et al., Sov.J.Nucl.Phys. **38**, 1205 (1983).

[69] S.I. Bityukov et al., *Phys. Lett.* **B188**, 383 (1987).

[70] M. Atkinson et al., *Nucl. Phys.* **B231**, 1 (1984).

[71] Yu.M. Antipov et al., Pis'ma JETF **38**, 356 (1983).

[72] Valery Kubarovsky, $\phi\pi$ Photoproduction and Search for Exotic Meson with CLAS, CLAS-ANALYSIS Note 2000-001.